THE ABUNDANCE OF HELIUM RELATIVE TO HYDROGEN IN THE ORION NEBULA

Thesis by

John Samuel Mathis

In Partial Fulfillment of the Requirements

For the Degree of

Doctor of Philosophy

California Institute of Technology

Pasadena, California

1956

ACKNOWLEDGMENTS

The author wishes to acknowledge the constant encouragement and guidance of Dr. Donald E. Osterbrock, who suggested the problem and supervised the work leading to this thesis. Dr. Guido Munch contributed many valuable suggestions and criticisms. Dr. William Tobocman performed a very valuable sample calculation of one of the matrix elements appearing in Chapter IV. The author's wife, Mrs. Carol S. Mathis, and Mr. John T. Harding, Jr., assisted in assembling the thesis. Finally, the author is grateful for the financial support received from the National Science Foundation during the course of the thesis work.

ABSTRACT

Spectrograms were taken at two slit positions in the brighest portion of the Orion Nebula near the exciting star θ' Ori C. Four independent measurements were made in each slit position of the ratios of the He I lines λλ4027, 4471, and λ5876 to the hydrogen lines H , H , and H , respectively. The ratios of the [OIII] lines λ4959 and λ4363 and of the [OII] lines λ3726 and λ3729 were also determined. Reddening by interstellar absorption was taken into account.

The electron density was found from the [OII] lines to be 3,800 $cm.^{-3}$ The electron temperature was found from the [OIII] lines to be 10,000°K. The theory of statistical equilibrium was developed for neutral helium, and from the three helium lines the ratio of abundances of helium and hydrogen was found to be 0.128 by number. All three lines gave results within nineteen per cent of the average in both slit positions.

It was found that the absorption of the line of He I at λ3889 in the spectrum of θ' Ori C could take place in only .025 parsec under the most favorable conditions.

In order to estimate the lifetime of the 2^3S level in helium the probability of two-photon emission was estimated. The estimate was $P = 1.1 \times 10^{-5}$ $sec.^{-1}$

TABLE OF CONTENTS

Chapter I. The Problem of Elementary Abundances in Nebulae

A. Abundance Investigations in Nebulae.

Astrophysicists have devoted much effort towards determining the composition of practically all types of astronomical objects which are observable from the earth. Although hydrogen and helium are by far the most plentiful elements in the universe, the ratio of their abundances is very difficult to determine directly and is consequently very poorly known. While the ratio of the two elements' abundances can be inferred through models of stellar interiors, where the helium abundance enters as a parameter, direct determinations must depend on measurement of the radiation which has been emitted or absorbed by helium atoms. Unfortunately, even the first excited state of helium has a very high excitation potential. The only astronomical objects which are hot enough to cause an appreciable number of surface helium atoms to be excited are the spatially rare O and B stars or other even less common stars of the same surface temperature class.

The study of the helium to hydrogen ratio in the hot stars themselves is complicated by both theoretical and observational difficulties. The theoretical uncertainties are inherently great because the observed line strength depends in a complicated way upon the poorly known march of pressure, temperature, and turbulent velocity in the stars' outer layers. The method of transfer of the line radiation, that is, the ratio of absorption to scattering of the line radiation as a function of depth in

the atmosphere, influences the abundance results also.

Observationally, the principal difficulty in stellar helium abundance determinations is that most of the radiation of a hot star and all of the strong resonance lines of both helium and hydrogen lie in the portion of the spectrum which is absorbed by the earth's atmosphere. The observable portion of the spectrum is merely the red tail of the stellar energy distribution function.

Gaseous nebulae, which are clouds of interstellar gas heated to incandescence by nearby hot stars, present one great advantage over the stars in regard to determining the helium to hydrogen ratio; practically every photon of helium line radiation in the observable region of the spectrum can escape from the nebula without undergoing successive scatterings and absorptions. Since the self-absorption of the nebula is low to visible lines, the number of atoms giving rise to a line is proportional to the strength of the line. One has to consider neither the frequency dependence of the opacity as for stars nor the transport of energy by convection.

Determinations of abundances in nebulae suffer from one complication more than do those in stars; there is almost always in the immediate vicinity of both hot stars and nebulae a considerable amount of dust which absorbs blue radiation selectively. The equivalent widths of absorption lines in stars are not affected, but the comparison of lines of widely different wavelength in the nebula is made more difficult by the reddening effect of the dust.

The brightest gaseous nebula as seen from the earth is NGC 1976, the Orion Nebula. It is located in the same spiral arm of the galaxy as our sun and is about five hundred parsecs [1] from the sun.

There have been a number of previous spectrophotometric investigations of the Orion Nebula in the past. Greenstein and Henyey [2,3,4] investigated the spectrum of the nebula and the variations in the character of the emission as a function of distance from the exciting stars. They estimated the electron temperature from the continuous Balmer emission. Wyse [5] made an extensive study of ten gaseous nebulae, the Orion Nebula among them, and made visual estimates of the line strengths of all the nebular lines. Greenstein [6] later found that the Balmer discontinuity is abnormally small in Orion; he suggested that reflection by dust might be the explanation.

Photographic investigation of the Trapezium stars by Baade and Minkowski [7] indicated that the reddening in the Orion Nebula might not be the same as the reddening of stars in the general field. Photoelectric investigations by Stebbins and Whitford [8,9] seemed to confirm this conclusion. The abnormality is in the sense that yellow light is extinguished more in the Trapezium stars than in the general field for a given absorption difference of blue and infrared radiation.

B. Physical Conditions in Gaseous Nebulae.

Gaseous nebulae have long been understood to be the results of the ionization of interstellar gas, which is mostly

hydrogen, by very hot, early-type stars either within the nebula or close by it. The dependence of the degree of ionization upon distance from the exciting star can be found qualitatively by means of an argument whose correctness has been shown by calculations [10].

The ionized material in the gaseous nebula is almost transparent and the neutral gas quite opaque to the ionizing radiation from the star. The radiation will therefore stream outward from the star relatively unhindered through the ionized material until it reaches the radius within which radiative ionizations just balance recombinations. At this radius there can exist some neutral material for which there is no ionizing radiation available. The neutral material absorbs the remaining high-energy radiation within the relatively short mean free path of photons in the neutral material. Hence the hot star, if immersed in material of uniform density, should be surrounded by a sphere of ionized hydrogen with a fairly sharp boundary. Actual nebulae rarely appear to be spheres, but they have very obvious density fluctuations.

The magnitude of the average time between collisions for a particle has important bearing on the physical state of the material in the nebula. Bright gaseous nebulae appear to have densities ranging from hundreds up to perhaps ten thousand or more ions per cubic centimeter in Orion [11]. At a density of 10^3 ions/cm^3, the radius of the ionized sphere around an O5 star will be about one-half of a parsec. The mean free path for an electron between collisions with ions is about 3×10^{-6} parsecs, or one astronomical

unit, if the appropriate collisional cross-section is 10^{-16} square centimeters. The time between such collisions, if electrons have a kinetic temperature of 10,000°K., is some 10^5 seconds, or roughly one day. It should be kept in mind that radiation is so diluted at a typical point in the nebula (a factor of 10^{-14} or so arising from the geometry of the situation) that radiative ionizations of a neutral atom are also infrequent and take place only after several hours in the outer portions of the nebula. Ionizations are dominant only because of the low probability of recombining collisions.

The character of the radiation emitted from the nebula is greatly influenced by the tenuity of the nebular material. All ions capture electrons and emit their characteristic recombination spectra, but the recombination lines of hydrogen and helium are most conspicuous because of the great predominance of these atoms numerically. Some ions in the ground state are excited collisionally by the low-energy electrons in the nebula and make a radiative transition back to the ground state. It so happens that all of the low-lying levels of the abundant ions of oxygen, sulfur, nitrogen, and argon are metastable with radiative lifetimes of the order of seconds. An excited ion practically never suffers a second collision within this time and therefore almost always makes a radiative transition to the ground state with the emission of a forbidden-line photon.

It is easy to see qualitatively why the populations of the various levels of hydrogen and helium differ from the distributions expected in equilibrium. Most atoms are ionized in the

nebula, but when recombination does occur, the atom drops to the ground state or to a metastable level in the time required for a series of optically allowed transitions. In this time the probability of the atom being disturbed by a second collision is negligible. The atom then remains in the ground state until it suffers re-ionization minutes or hours later. Transitions between excited states and collisional excitations of the ground states of hydrogen and helium are exceedingly improbable because of the energies required. Hence the excited levels are populated only by very rapid radiative cascading down to the ground state or by infrequent radiative excitations from the ground state. There is therefore a vastly greater concentration of the neutral atoms in the ground state than there would be if the system were in equilibrium (i.e., if the radiation energy distribution and energy density corresponded to the same temperature).

The velocity distribution of the charged particles in the nebula can be shown [12] to be Maxwellian and can therefore be characterized by an electron temperature Te. The Maxwellian distribution is established because elastic collisions between charged particles due to long-range Coulomb forces greatly outnumber inelastic collisions between pairs of ions and electrons. The temperature of the distribution is determined by a balance between the rate of gain of kinetic energy of electrons due to photo-ionizations and the loss of kinetic energy due to the radiation of the recombination spectra of hydrogen and helium and the forbidden lines from the collisionally excited metastable levels of other ions.

C. Determination of the Abundance of Helium Relative to Hydrogen.

The abundance of helium relative to hydrogen in a gaseous nebula can be determined from the line strengths of the recombination spectra of the elements if the line emissivity per unit volume can be related to the total atomic densities and also if the path length of material producing helium line radiation along the line of sight can be related to the total path length for hydrogen emission.

The relation of the path lengths for helium and hydrogen has recently been considered by Swihart [13]. His calculations show that the radii of the spheres of ionized helium and hydrogen are virtually identical for stellar temperature above 40,000°K. or abundances of more than four hydrogen atoms to one helium atom. These conditions are probably well fulfilled in nebulae. Incidentally, if there were an appreciable difference in the radii of the ionized zones, the ratio of the zone sizes might be used for a relative abundance determination.

The relation of the emissivity per unit volume to the total atomic populations can be determined theoretically with the aid of the assumption that the populations of each atomic level remain constant in time, so that the rate of transitions into the level from upper levels can be equated to the number of transitions downward to lower ones. In some cases transitions upwards from lower levels may be important also.

The theory for hydrogen has been carried out [14,15]; computations by Menzel and his associates at the Harvard College Observatory [15] are the most complete. The computations for

helium have been performed rather approximately [16], but recomputation to a higher degree of accuracy was necessary for the present investigation.

The metastability of the 2^3S in helium is one source of complication of the calculations of level populations. If the metastable level is so long-lived that the number of atoms leaving it by radiative ionizations per second is comparable to the number leaving by superelastic collisions or radiative transitions to the ground state by two-photon emission, the radiative and collisional excitations from this level to the lower excited triplet states may be quite important. Hence the probability of two-photon emission and collisional de-excitation of the 2^3S level must be computed before we can safely neglect the effects of excitations from this level to the higher levels.

The electron temperature affects the rate of recombination into various levels differentially, and some estimate of it is necessary for the theory. Fortunately such an estimate is possible because the OIII ion has two low-lying metastable levels with different excitation potentials. The upper level makes a transition to the lower one with the emissions of λ 4363, and the lower level makes transitions to the ground state with the emission of the strong "nebulium" lines $\lambda\lambda$ 4959, 5007. The populations of the levels can be determined by the strengths of the lines and can also be related to the electron temperature by calculations of cross-sections of collisional excitations as functions of electron temperatures [17].

For the present investigation, the strengths of the nebular lines from λ 3700 to λ 6900 were observed in two bright portions of the Orion Nebula. Both positions were quite close to the Trapezium stars. The observed line intensities had to be corrected for the reddening effects of absorption. The reddening of the Trapezium stars as determined photoelectrically [8,9] was applied to the observed nebular lines.

Finally, the population of the metastable 2^3S level in helium, which had been computed in the course of the determination of abundance ratio of helium to hydrogen, was used to predict the strength of the absorption line at λ 3889 in the spectrum of the Trapezium stars. The prediction was compared with observation of the line by Wilson [18].

Chapter II. Observational Determination of Line Strengths

A. Observational Procedures.

The strengths of the nebular emission lines were determined at two slit positions in the Orion nebula. These positions are marked in figure 2.1. The slit in both cases subtended 99" of arc. Position E' was centered upon a faint (twelfth magnitude) star which is 0.4' almost due south from θ^1 Orionis C. Position B' extended eastward from θ^1 Orionis C with its end due south of θ^1 Orionis D. Both of the positions are in the brightest region of the nebula. For the present investigation, spectrograms in the blue and red regions of the spectrum were obtained with the Cassegrain spectrograph of the 60" reflector at the Mount Wilson Observatory. The F/1 camera of four inch focal length was used throughout the program.

The spectrum from λ3700 to λ5100 was photographed on Kodak IIa-J plates baked two days at 50°C. In this spectral region a 15,000 line-per-inch grating, blazed at λ3500 in the second order, provided a dispersion of 81 Angstroms per millimeter.

Slit widths of four and five hundred microns were used on the blue plates, which gave projected widths of twenty-five and thirty-one microns on the plates. With the narrower slit width, lines three Angstroms apart could be resolved. A comparatively wide slit was used so that the line profile would be rather flat on top and therefore less sensitive to fluctuations of the plate grain than would a narrow line. Furthermore, the background is brought up more quickly with a wide slit. The

length of the longest exposures on blue plates was adjusted to bring the background up to a photometerable level so that its contribution to the nebular lines λ4027 and λ4363 could be evaluated. Hence, strengthening the background relative to the lines was desirable. The limitation on slit width was that the mercury line at λ4358 had to be separable from [O III] λ4363. The mercury line is strong in the sky over Mount Wilson because of lights in nearby cities.

A succession of exposure times for the blue plates was selected with the strongest nebular lines of interest, H_β and [O III] λ4959, near the upper limit of usable intensity on the shortest exposure. Succeeding exposure times were such that the weakest measurable lines on each plate became the strongest measurable lines on the next plate, until the least intense emission of interest, the background near the weak lines λ4363

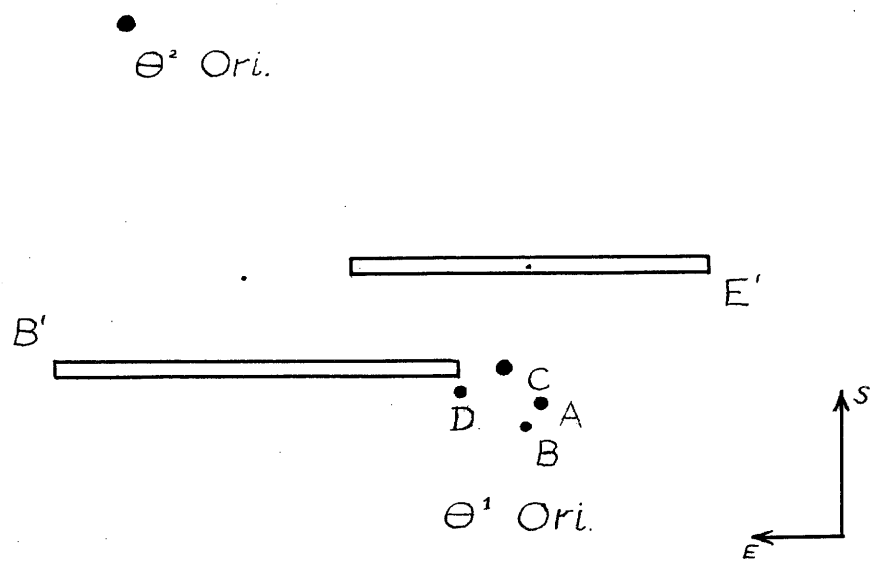

Figure 2.1. The locations of the slit settings E' and B' relative to the stars in θ^1 Onionis.

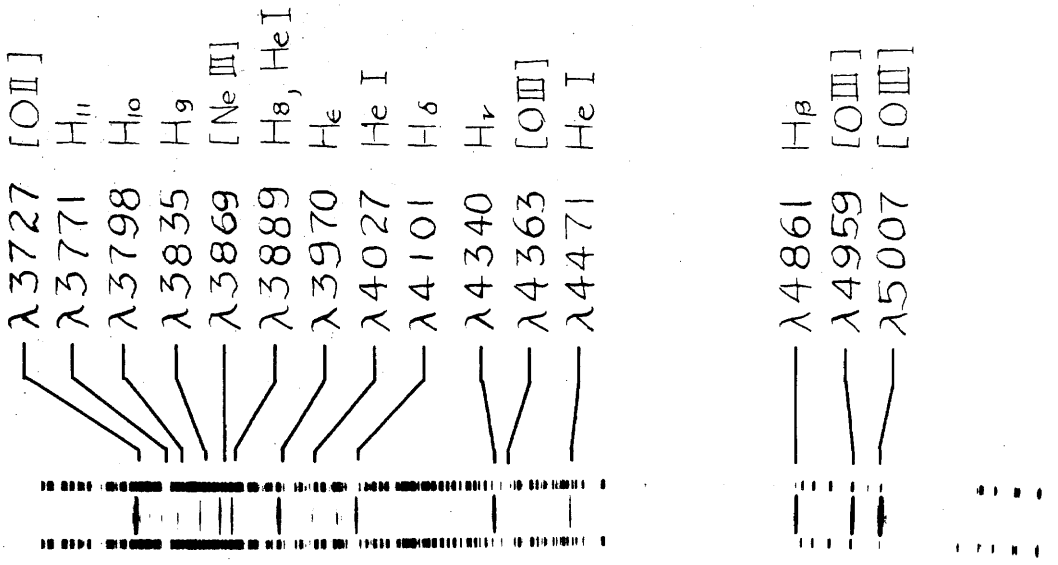

IIa-J Emulsion, 90 Minute Exposure, Position E'

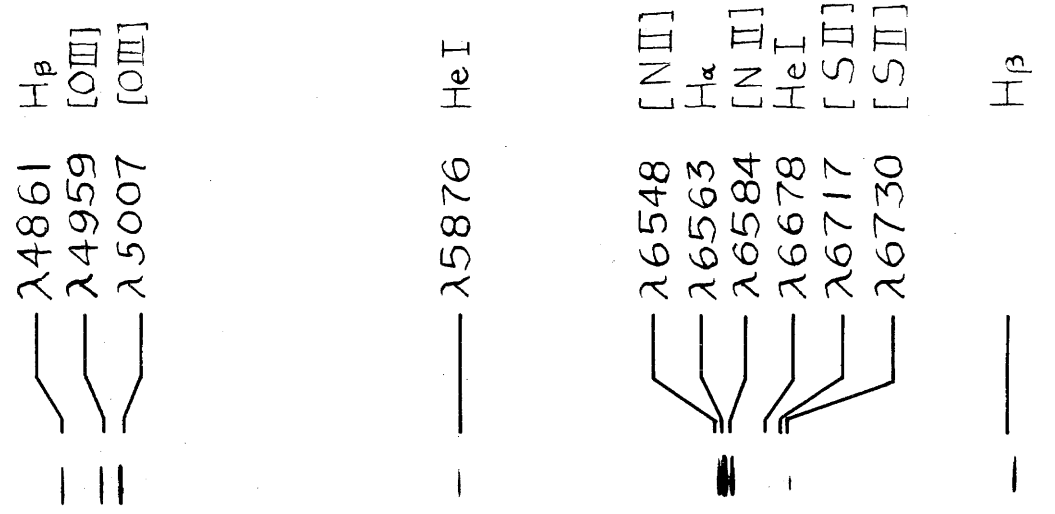

103a-F(3) Emulsion, 12 Minute Exposure, Position B'

Figure 2.2. Reproductions of typical spectrograms obtained in the investigation.

and λ4027, was at the lower limit of intensity on the longest exposure. The actual exposure times in a typical series of plates were seventy seconds, and three, nine, twenty-five, and eighty minutes.

Spectrograms covering the interval λ4600 - λ6800 were taken on unbaked 103a-F(3) plates. The red plates were taken at a slit width of eight hundred microns, which was projected to fifty microns on the plates. Probably lines separated by six Angstroms could have been resolved.

Only one exposure time, five minutes, was sufficient in the red region to obtain the only lines of interest, H_β and He I λ5876, in measurable strengths. This was primarily because H_β appeared in both the second and third orders on the plates, and the weaker of these images (the second order one) was only twice as strong as λ5876.

Slit lengths of twelve millimeters, which projected to 0.75 millimeters on the plates, were used with both emulsions.

Four series of spectra in the blue region were taken for each slit position. An attempt was made to take only one series on either position on any single night to make any systematic errors, such as sky illumination by the moon or city lights, more obvious. Two sets of blue spectra of the position E' were obtained on one night.

Five of the seven usable red spectra were obtained in one night and the remaining two on one other night.

Comparison spectra of several G2 V stars were taken in both spectral regions with the same optical arrangement as was

used on the nebula. By comparison of the G2 V spectrograms with the solar energy distribution, the wavelength sensitivity of the entire optical system and the atmosphere of the earth could be determined within an arbitrary factor. No attempt was made to take the comparison and nebular spectrograms at the same zenith distance. The errors introduced by wavelength-dependent extinction in the difference in air paths of the nebular and comparison star spectra are smaller than other photometric errors.

No filters were used on the blue spectrograms because overlapping orders from the grating did not affect the region of interest on the spectrograms. The emulsion was insensitive to the first-order red and infrared spectrum. The third order ultraviolet spectrum was primarily cut off by atmospheric extinction. The possibility that the region of $\lambda 5000$ on the comparison star plates was being contaminated with the third-order ultraviolet at $\lambda 3300$ was investigated. Several spectra of the G stars were taken with a Wratten #1A gelatin filter in the optical train. The transmission of the filter is essentially zero below $\lambda 3800$ and uniform at 85% above $\lambda 4300$. The comparison star plates taken with the filter showed no weakening of the $\lambda 5000$ region relative to shorter wavelengths, so the overlapping third order must have indeed been negligible at all wavelengths.

The transmission of the Wratten #1A filter was measured directly with a Beckman spectrophotometer. The spectra of the comparison stars with and without the filter gave an independent means of determining the transmission of the filter. Unfortunately, comparison of the two means of measurement gave indeterminate

results. The photographically determined transmission was uniform at wavelengths greater than 4300 Angstroms but fell to values at λ4085 and λ4030 that the measured transmission gave at λ4135 and λ4070 respectively. The wavelength scale of the Beckman spectrometer was not accurate to within 50 Angstroms, so the test of the photometry was inconclusive.

A filter was necessary on exposures in the red region to eliminate contamination of the comparison spectra by overlapping third and fourth orders. A Wratten #3 gelatin filter, which has a transmission dropping to zero very quickly blueward of λ4800, was used. The lines H_β and [O III] λ4957, λ5007 appeared on the nebular plates in both the second and third orders, but only one order appeared at any given point on the plate. The emulsion sensitivity made the first order infrared spectrum unimportant.

The five comparison star spectra in the blue were obtained on three different nights. Three other spectra were taken in the blue with the Wratten #1A filter in the optical train. Five comparison spectra in the red were obtained, all taken the same night.

A knowledge of the relation between the blackening on a photographic plate and the intensity of light producing the blackening is necessary for photographic photometry. This relation, a plot of which is called the characteristic curve, was determined by use of the calibration optics of the coudé spectrograph of the 100" telescope at Mount Wilson Observatory. The calibration and nebular plates were always taken from the same box and developed together. For the IIa-J emulsion, calibrations were

taken at wavelengths of 4200 and 4800 Angstroms. For the 103a-F(3) emulsion they were taken at about 4900 and 6400 Angstroms. The technical data for the calibration plate exposures are given in Appendix A.

A series of calibration plates with increasing exposure times was taken for each night's work. Each nebular plate could be compared with at least one calibration plate exposed within a factor of two times as long. Reduction of the results of the calibration plates after the observing program was completed brought to light a flaw in the procedure used; on the IIa-J emulsion the characteristic curve for λ4800 radiation had definitely a steeper slope than did the λ4200 curve. The shape of the curve did not change significantly with exposure time. The calibrations should therefore have been made at several wavelengths instead of just two, but not necessarily at more than one or two exposure times. Figure 2.3 shows the actual difference found. The curves found on 103a-F(3) emulsion at λ4800 and λ 6600 were practically identical in shape.

The characteristic curves did show a slight variation with development, as shownin figure 2.3. Hence it is necessary either to control conditions of development very carefully or to develop calibration plates with the plates to be calibrated. The characteristic curves of calibrations cut from different boxes of plates and consequently baked separately seemed no more different than were curves of plates from the same box that were developed separately. Unfortunately calibrations from different boxes were never developed together.

An attempt was made to determine the variation of the shape of the characteristic curve with wavelength after the actual nebular observations had been completed. Dr. G. Münch kindly obtained additional calibration exposures with the wavelength ranging continuously from $\lambda 3500$ to $\lambda 4800$ on IIa-J plates and from $\lambda 4800$ to $\lambda 6600$ on 103a-F(3) plates. These plates unfortunately did not definitely establish the variation of the characteristic curve with wavelength. Values of the slope of the curve on the linear portion fail to define a smooth curve when plotted against wavelength, as shown in figure 2.4. It was finally decided to use the curve taken at $\lambda 4200$ for all wavelengths short of $\lambda 4250$ and the $\lambda 4800$ curve for wavelengths $> \lambda 4300$. Figure 2.4 shows that this procedure is fairly appropriate to the resolution of the problem. Fortunately, the color dependence of the curve is not great enough to affect the photometric work to a vital degree in any case.

In the months of September and October, calibration plates were taken with two tube sensitometers at the Mount Wilson Observatory. The results obtained with each instrument were considered inferior to those obtained with the coudé optics of the 100" telescope. The tube sensitometers showed such a scatter of points that the characteristic curve obtained from the results was ambiguous. Wavelength variations with the tube sensitometer could be achieved only by the use of filters. It was much less convenient to use the coudé optics than a tube sensitometer; frequent trips between the 60" and 100" telescopes were necessary, and occasionally the observer using the 100" telescope was inconvenienced.

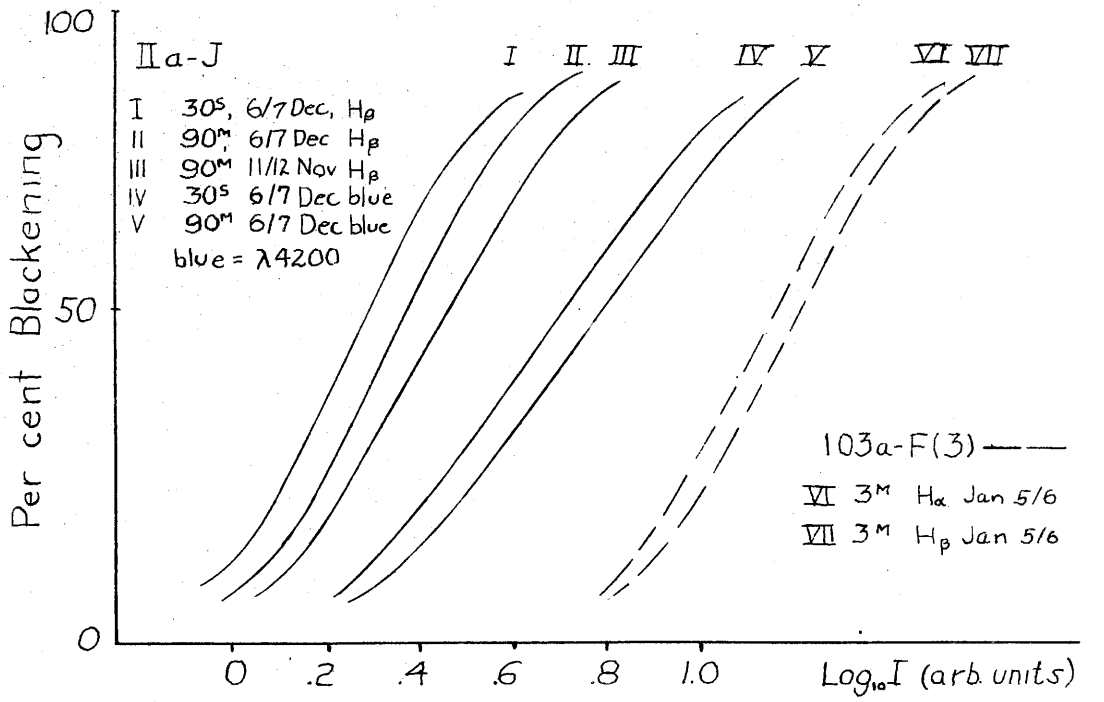

Figure 2.3. Typical characteristic curves obtained at different exposure times and wavelengths on the two emulsions.

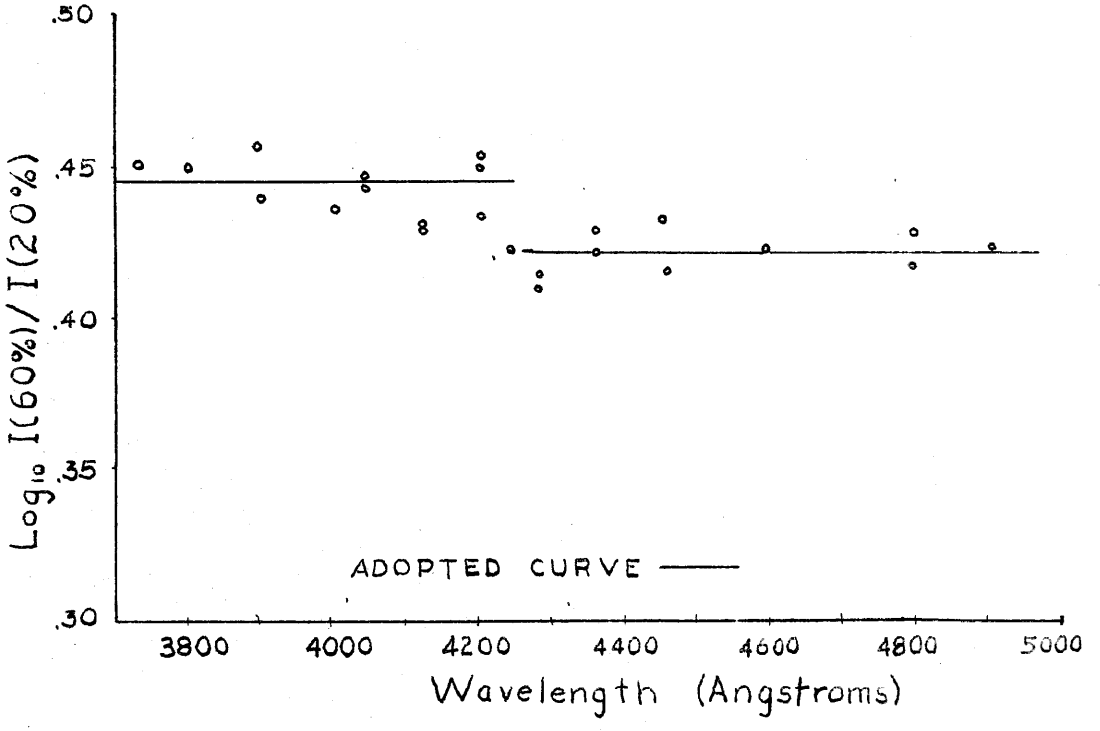

Figure 2.4. The slope of the characteristic curve as a function of wavelength. The slope was taken as the ratio of intensities producing blackenings of twenty and sixty per cent..

Rather standard development procedure was employed. All of the nebular and comparison star plates of each night's observations were developed together with the appropriate calibration plates. The mechanical rocker in the darkroom in the 60" telescope dome was used. The 103a-F(3) emulsion plates were developed 4.5 minutes in D-19 developer at 68°F.; the IIa-J plates, 13.5 minutes in D-76. An acid short-stop and separate fixing solution were used in a conventional manner.

B. Reduction of the Spectrograms.

Most of the useful spectrograms and calibration plates were traced on the Sinclair Smith recording microdensitometer at the California Institute of Technology. Tracings were made at a magnification of four hundred and fifty for the nebular and comparison star spectra and of thirty-eight for the calibration plates. Typical tracings are shown in figures 2.5 and 2.6.

The Sinclair Smith instrument gave a deflection to the recording pen proportional to the amount of light the plate transmitted. Measurements on nebular lines were expressed by subtracting from one the ratio of the amounts of light transmitted by the image of the line and the unexposed portions of the plate. The subtraction of the ratio from one made the reading of a weak line be close to zero. This measure, expressed in percentage, will be called the blackening of a line.

A few of the spectrograms were traced on the direct-intensity microphotometer at the Mount Wilson Observatory. It was impossible to make use of the direct-intensity feature of the

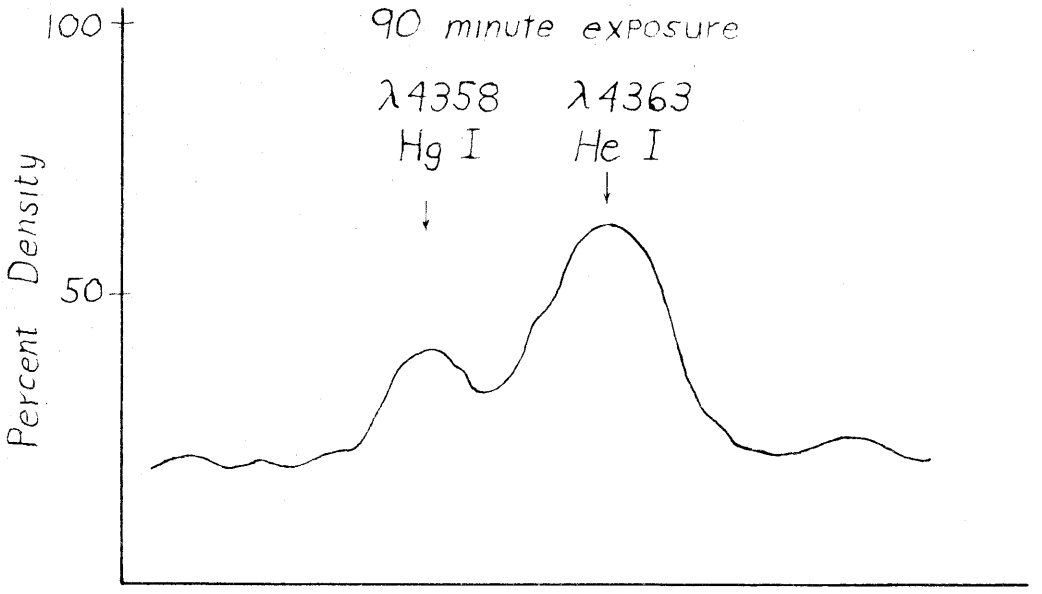

Figure 2.5. Tracing of the lines λ4358 of mercury and λ4363 of [O III].

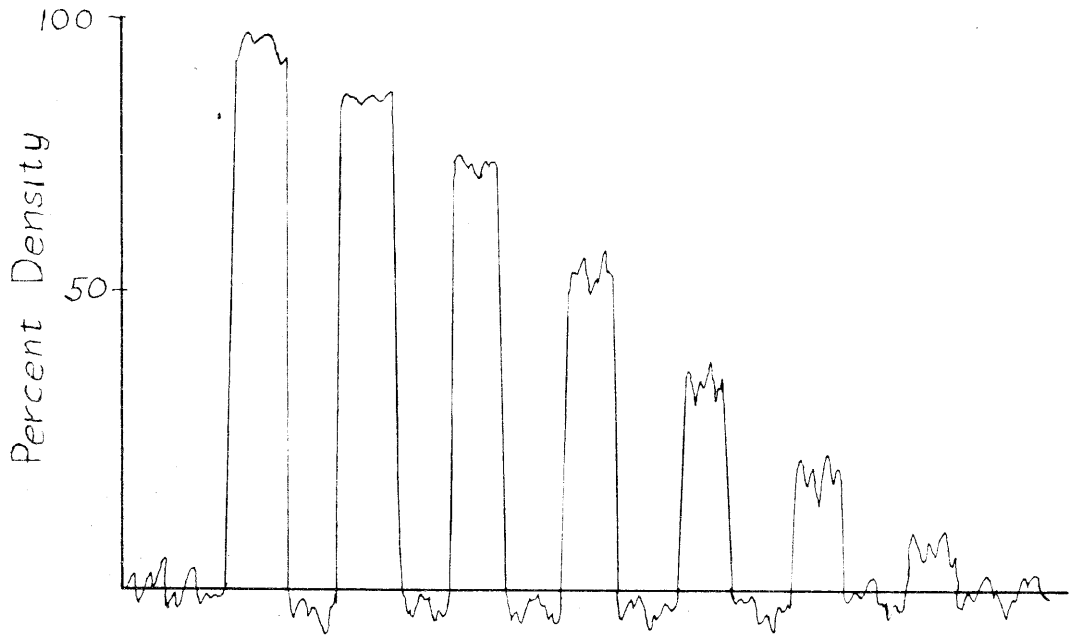

Figure 2.6. Tracing of a typical calibration plate (coudé 68).

instrument because wedge calibrations would have been needed. The instrument gave a deflection that was not proportional to the blackening but was a monotonic function of it. The readings on the two instruments can be compared only after the line intensity ratios are determined.

Several nebular plates and their calibration were traced on both instruments. The line intensities measured on plate xf 1089, uncorrected for effects of emulsion sensitivity, are compared in Table 2.1. The intensity of H_{11} is taken as unity for each tracing.

Table 2.1. Comparison of Microdensitometers at Mount Wilson Observatory and C.I.T.

Line	$\log_{10}$ Intensity (C.I.T.)	$\log_{10}$ Intensity (Mount Wilson)
He I λ4471	+0.236	off scale
He I λ4027	- .044	- .050
H_9	- .266	off scale
H_{10}	+ .146	+ .134
H_{11}	0.00	0.00
H_{12}	- .067	- .060
H_{13}	- .149	- .160

The table shows that these are no large systematic errors in the readings between the two instruments. The Mount Wilson instrument was not used successfully over as large a range of blackening as was the one at C.I.T. This feature is illustrated by the two lines which were off scale on the one and quite usable

on the other.

The reproducibility of the measurements of either instrument was fairly high. The Sinclair Smith instrument gave readings of the density of a given line which varied within about two per cent of the clear-plate-to-dark reading. Sometimes the readings were taken months apart. The Mount Wilson instrument was only tested for variability over a period of one day but gave about the same performance. The readings were also independent of the direction of tracing.

The procedure used in deriving from the tracings the intensity of the nebular emission as seen from outside the earth first involved determination of the characteristic curves from the calibration plates. The characteristic curve was assumed to be known for all wavelengths as explained in Section A of this chapter.

In the following discussion of the method used to determine line intensities from the tracings, we will need to appeal to an empirical law of photography. The blackening on a photographic plate is given by an expression of the form

$$B = B_{\lambda}(x), \tag{2.1}$$

where

$$x = A(\lambda)\, E(\lambda)\, f(t). \tag{2.2}$$

Here B is some numerical expression of the blackening on the plate, such as that given by the microdensitometer tracings. The B_{λ} on the right of equation 2.1 denotes a functional relation, perhaps dependent on the wavelength λ and exposure time t, between B and the quantity x. The B_{λ} was found by calibration

to depend somewhat on λ and not on t. $A(\lambda)$ is a quantity, defined later, that depends only on λ. The $E(\lambda)$ is the flux of energy of wavelength λ that falls on the plate per unit area and time. $E(\lambda)$ is taken to be constant in time for our purposes. The function f of the exposure time t gives the dependence of the blackening properties of the light on time.

It might be supposed that only the total amount of light striking the plate, $E(\lambda)\cdot t$, would be important. In this case, $f(t) = t$. Such is not quite the case; $f(t)$ is better expressed in the form

$$f(t) = t^p \ , \qquad (2.3)$$

where p is independent of time and close to one. We will now make the assumption that p, and therefore the function f, is independent of λ. This assumption can be checked by plotting the logarithm of the $E(\lambda)$ required to produce a constant blackening in time t versus log t. Since at constant B x is held constant, the negative of the slope of the curve should be p. This was done for $\lambda 4800$ and $\lambda 4200$ on IIa-J emulsion. The results were $p(\lambda 4200) = 0.735$ and $p(\lambda 4800) = 0.785$. The assumption that $f(t)$ is independent of λ is equivalent to using the mean value of p for all wavelengths. It should be mentioned that the values of $p(\lambda)$ given above are not very reliable. The values of $E(\lambda)$ plotted were subject to errors due to fluctuations in the brightness of the coudé light source caused by variations in line voltage.

The quantity $A(\lambda)$ will be defined in the following way:

Let $E^*(\lambda)$ be the intensity required to blacken the plate to a value B_o in a given time t_o. Then, for all λ,

$$B_\lambda [A(\lambda)\, E^*(\lambda)\, f(t_o)] = B_o \,. \qquad (2.4)$$

Now the restriction is made that for the blackening B_o the variation with λ on the left side of equation 2.4 will be only in the product $A(\lambda)\, E^*(\lambda)$. Then

$$A(\lambda)\, E^*(\lambda) = \text{constant} = C, \qquad (2.5)$$

since the right side is independent of λ. The value of the constant is immaterial for relative photometry. The quantity $A(\lambda)$ is by definition inversely proportional to the amount of energy $E^*(\lambda)$ required to produce a given blackening, so it is natural to associate it with the sensitivity of the plate to light of wavelength λ.

The characteristic curves of an emulsion are plots of B versus $\log_{10} E(\lambda)$ at constant t, and thus are graphs of the function $B_\lambda(x)$. The definition of $A(\lambda)$ is equivalent to making the characteristic curves for various wavelengths pass through the same point at the blackening B_o.

Let us consider what intensity $E'(\lambda)$ will be required to produce a blackening of B_o in time t. The blackening B_o will be produced whenever the function $B_\lambda(x)$ has the same argument as it does in equation 2.4. Hence we find $E'(\lambda)$ by equating the argument x at time t to the value of x in

equation 2.4, and get

$$E'(\lambda) = E^*(\lambda)\, f(t_o)/f(t). \qquad (2.6)$$

The energy flux of the Orion Nebula will be denoted by $E_{neb}(\lambda)$. Suppose a nebular plate exposed for time t has a line at λ_1 with a blackening $B_{neb}(\lambda_1, t)$. We can use the characteristic curve to give the ratio of the parameters x that correspond to blackenings of B_{neb} and the reference blackening B_o. This known ratio will be called $R(t, \lambda)$, given by

$$R(t, \lambda) = \frac{A(\lambda)\, E_{neb}(\lambda)\, f(t)}{A(\lambda)\, E'(\lambda)\, f(t)}. \qquad (2.7)$$

But, by equations 2.5 and 2.6, the denominator of $R(\lambda, t)$ is

$$A(\lambda)\, E'(\lambda)\, f(t) = A(\lambda) E^*(\lambda)\, f(t_o) = C\, f(t_o). \qquad (2.8)$$

If we find $R(t, \lambda_1)$ and $R(t, \lambda_2)$ for two lines on the same plate, the ratio $R(t, \lambda_1)/R(t, \lambda_2)$ will give

$$\frac{R(t, \lambda_1)}{R(t, \lambda_2)} = \frac{A(\lambda_1) E_{neb}(\lambda_1)\, f(t)}{C\, f(t_o)} \cdot \frac{C\, f(t_o)}{A(\lambda_2)\, E_{neb}(\lambda_2)\, f(t)}$$

$$= \frac{A(\lambda_1)\, E_{neb}(\lambda_1)}{A(\lambda_2)\, E_{neb}(\lambda_2)}. \qquad (2.9)$$

If we wish to compare lines on different plates (with exposure times t_1 and t_2), we must use one or more lines which are measurable on both plates. We form the ratio $R(t_1, \lambda)/R(t_2, \lambda)$, which can be written as

$$\frac{R(t_1, \lambda)}{R(t_2, \lambda)} = \frac{A(\lambda)\, E_{neb}(\lambda)\, f(t_1)}{A(\lambda)\, E_{neb}(\lambda)\, f(t_2)} = \frac{f(t_1)}{f(t_2)}. \qquad (2.10)$$

The ratios for all such measurable lines can be averaged, since $f(t_1)/f(t_2)$ is assumed to be independent of λ. If the variations in the quantity p of equation 2.3 were known, they could be taken into account in the averaging.

The ratio of two nebular lines which appear in measurable strengths only on different plates can now be found. The quantities $R(\lambda,t)$ for each line can be found. Their ratio is

$$\frac{R(t_1, \lambda_1)}{R(t_2, \lambda_2)} = \frac{A(\lambda_1)\, E_{neb}(\lambda_1)\, f(t_1)}{A(\lambda_2)\, E_{neb}(\lambda_2)\, f(t_2)}, \qquad (2.11)$$

and the average $f(t_1)/f(t_2)$ obtained by applying equation 2.10 to as many lines as possible can be used.

The equations 2.9 and 2.11 involving $E_{neb}(\lambda)$ and the known quantities $R(t,\lambda)$ also involved $A(\lambda)$. However, if we write exactly analagous equations for the comparison star plates instead of the nebular ones, we can substitute known values for the solar energy fluxes to obtain equations involving $A(\lambda)$ alone. From these equations $A(\lambda)$ can be determined, and equations 2.9, 2.10, and 2.11 give the desired nebular intensities $E_{neb}(\lambda)$.

A listing of the nebular plates used in the investigation is given in Table 2.2. Some of the ratios $R(t,\lambda)$ are marked with an asterisk to denote that the ratio should be given a weight of one-half in averages because the blackening of the line corresponded to a point somewhat off the linear portion of the characteristic curve. The blackening B_o was chosen to be 50% density on tracings with the Sinclair Smith microdensitometer.

For the two tracings of blue plates that were performed with the Mount Wilson photometer, a B_o of 2.52 inches above the clear plate pen deflection was used. The two were matched to represent the same intensity by a comparison of tracings made on the two machines.

From the values listed in Table 2.2 we can find the functions $f(t_1)/f(t_2)$ for any two plates with common lines regardless of the nights on which they were taken. However, only plates taken in a series on a single night were reduced together. The final line ratios derived from each of the four series were then averaged together. The ratios of H_β and He I λ5876 as obtained from the individual red plates were averaged.

From the data given in Table 2.2 the ratios $f(t_1)/f(t_2)$ for each pair of plates can be found by equation 2.10, and the line intensity ratios uncorrected for plate sensitivity by equation 2.11. We will consider one series of spectra in some detail as an illustrative example. Only final results will be given for the other series.

Let us consider the series taken 9/10 December, 1955, on position B'. Table 2.3 gives the average value for $\log_{10} f(t_1)/f(t_2)$ for each pair of successive plates and the average deviation of the individual values of $\log_{10} R(t_1,\lambda)/R(t_2,\lambda)$. The probable error σ as computed from the standard formula of probability theory is also given. Probably the main source of internal deviations on an individual night is the random errors introduced by photographic grain, so the probable error has some

Table 2.2. Nebular Emission Lines on IIa-J Plates

IIa-J Emulsion
(Ratios marked * given half weight in averages)

Plate, Date, Exposure, Filter	Line or Background of Line	$\text{Log}_{10} R(\lambda,t)$	Plate, Date, Exposure, Filter	Line or Background of Line	$\text{Log}_{10} R(\lambda,t)$
		Position B'			
xf 913	λ3869	+ 1.05	xf 915	H_ϵ	- .035
7/8 Dec.'55	H_8	+ .242	7/8 Dec.'55	H_δ	+ .355
80 min.	λ4027	+ .067	9 min.	λ4471	- .150
Wratten 1A	b(4027)	- .430	Wratten 1A		
	λ4363	+ .050			
	b(4363)	- .220	xf 916	H_δ	+ .040
	λ4471	+ .387	7/8 Dec.'55	H_γ	+ .280
	b(4471)	- .250	3 min.	H_β	+ .360
			Wratten 1A	λ4959	+ .030
xf 914	λ3869	-			
7/8 Dec.'55	H_8	- .080	xf 917	H_δ	+ .242
25 min.	H_ϵ	+ .275	7/8 Dec.'55	H_γ	+ .047
Wratten 1A	λ4027	- .229	70 sec.	λ4959	+ .018
	λ4363	- .200	Wratten 1A	H_β	+ .050
	λ4471	+ .115			

Table 2.2. Nebular Emission Lines on IIa-J Plates (continued)

Plate, Date, Exposure, Filter	Line or Background Of Line	Log_{10} $R(\lambda,t)$	Plate, Date, Exposure	Line or Background of Line	Log_{10} $R(\lambda,t)$
			Position B'		
xf 918	λ5007	+ .105	xf 927	H_{12}	- .198
7/8 Dec.'55	λ4959	- .315	9/10 Dec.'55	H_{11}	- .100
25 sec.	H_β	- .261	23 min.	H_{10}	+ .020
Wratten 1A	H_γ	- .290		H_9	+ .162
				λ3869	+ .440
xf 926	H_{12}	+ .106		λ4027	- .087
9/10 Dec.'55	H_{11}	+ .165		λ4363	- .112
80 min.	H_{10}	+ .260			
	λ4027	+ .116	xf 928	H_δ	+ .482*
	b(4027)	- .242	9/10 Dec.'55	H_ϵ	+ .164
	H_9	+ .407*	9 min.	λ3869	+ .079
	λ4363	+ .102		H_9	- .215
	b(4363)	- .215		H_8	+ .118
	λ4471	+ .443*			
	b(4471)	- .236			

Table 2.2. Nebular Emission Lines on IIa-J Plates (continued)

Plate, Date, Exposure	Line or Background of Line	Log_{10} $R(\lambda,t)$	Plate, Date Exposure	Line or Background of Line	Log_{10} $R(\lambda,t)$
		Position B'			
xf 929	λ3726	+ .185	xf 1086	λ4957	- .025
9/10 Dec.'55	λ3869	- .240	7/8 Jan.'56	H_β	+ .015
3 min.	H_8	- .282	70 sec.	H_γ	+ .021
	H_ϵ	- .170		H_δ	- .285
	H_δ	+ .062		λ3727	- .070
	H_β	+ .315		λ3729	- .342
	λ4959	+ .310			
			xf 1087	H_{10}	- .352
xf 930	λ3726	+ .058	7/8 Jan.'56	H_9	- .217
9/10 Dec.'55	λ3729	- .226	9 min.	H_8	+ .085
70 sec.	H_δ	- .208		λ3869	+ .065
	H_γ	+ .092		H_ϵ	+ .165
	H_β	+ .055		H_γ	+ .467*
	λ4957	+ .007		λ4471	- .217
xf 931	H_β	- .312			
9/10 Dec.'55	λ4959	- .342			
25 sec.	λ5007	+ .117			

Table 2.2. Nebular Emission Lines on IIa-J Plates (continued)

Plate, Date, Exposure	Line or Background of Line	$\log_{10} R(\lambda,t)$	Plate, Date, Exposure	Line or Background of Line	$\log_{10} R(\lambda,t)$
		Position B'			
xf 1088	λ 3727	+ .300*	xf 1090	H_{13}	+ .117
7/8 Jan.'56	λ 3729	+ .040	7/8 Jan.'56	H_{12}	+ .163
3 min.	λ 3869	- .210	90 min.	C_{11}	- .350
	H_8	- .193		H_{11}	+ .278
	H_ϵ	- .180		H_{10}	+ .360
	H_δ	+ .072		λ 4027	+ .222
	H_γ	+ .387		b(4027)	- .300
	H_β	+ .430		λ 4363	+ .070
	λ 4959	+ .407		b(4363)	- .290
				λ 4471	+ .505*
xf 1089	H_{13}	- .265		b(4471)	- .430
7/8 Jan.'56	H_{12}	- .183			
25 min	H_{11}	- .116	xf 1111	λ 3726	+ .270
	H_{10}	+ .030	8/9 Jan.'56	λ 3729	+ .033
	H_9	+ .140	3 min.	λ 3869	- .252
	H_8	+ .519*		H_8	- .238
	λ 4471	+ .519*		H_ϵ	- .192
	λ 4027	- .160		H_δ	- .077
	λ 3869	+ .120		H_γ	- .368*
				H_β	+ .417*
				λ 4959	+ .420*

Table 2.2. Nebular Emission Lines on IIa-J Plates (continued)

Plate, Date, Exposure	Line or Background of Line	$\log_{10} R(\lambda,t)$	Plate, Date, Exposure	Line or Background of Line	$\log_{10} R(\lambda,t)$
	Position B'			Position B'	
xf 1112	λ3726	+ .620*	xf 1114	H_{12}	+ .150
8/9 Jan.'56	λ3729	+ .360	8/9 Jan.'56	H_{11}	+ .290
9 min.	H_{11}	- .345	75 min.	H_{10}	+ .380*
	H_{10}	- .325		λ 4027	+ .210
	H_9	- .205		b(4027)	- .250
	H_8	+ .130		λ 4363	+ .056
	λ3869	+ .160		b(4363)	- .303
	H_ϵ	+ .192		λ 4471	+ .550*
	H_δ	+ .325		b(4471)	- .390
	λ4471	- .250		Position E'	
xf 1113	H_{12}	- .240	xf 782	H_{13}	+ .220
8/9 Jan.'56	H_{11}	- .165	14/15 Nov.'55	H_{12}	+ .288
20 min.	H_{10}	- .077	100 min.	H_{11}	+ .372
	H_9	+ .090		λ 4027	+ .302
	H_8	+ .420		b(4027)	- .125
	λ3869	+ .410		λ 4363	+ .202
	H_ϵ	+ .500*		b(4363)	- .160
	λ4027	- .203			
	λ4471	+ .053			

Table 2.2. Nebular Emission Lines on IIa-J Plates (continued)

Plate, Date, Exposure	Line or Background of Line	$\log_{10} R(\lambda,t)$	Plate, Date, Exposure	Line or Background of Line	$\log_{10} R(\lambda,t)$
			Position E'		
xf 783	H_{13}	- .157*	xf 786	H_{14}	+ .315
14/15 Nov.'55	H_{12}	- .095	14/15 Nov.'55	H_{13}	+ .257
22 min.	H_{11}	- .017	100 min.	λ4027	+ .380*
	H_{10}	+ .060		b(4027)	- .106
	H_9	+ .174		H_{12}	+ .317
	λ4027	- .117		λ4363	+ .230
	λ4363	- .187		b(4363)	- .110
	λ4471	+ .150			
			xf 788	H_{14}	- .110
xf 784	H_β	+ .045	14/15 Nov.'55	H_{13}	- .200*
14/15 Nov.'55	H_γ	+ .110	22 min.	H_{12}	- .100
70 sec.	H_δ	- .086		H_{11}	- .020
	λ3726	+ .030		H_{10}	+ .078
	λ3729	- .202		H_9	+ .165
				λ4027	- .085
xf 785	H_γ	+ .072		λ4363	- .303*
12/15 Nov.'55	H_β	- .197		λ4471	+ .110
30 sec.	λ3727	- .250			

Table 2.2. Nebular Emission Lines on IIa-J Plates (continued)

Plate, Date, Exposure	Line or Background of Line	Log_{10} R(λ,t)	Plate, Date, Exposure	Line or Background of Line	Log_{10} R(λ,t)
		Position E'			
xf 788	H_β	+ .040	xf 897	H_{10}	- .290
14/15 Nov.'55	H_γ	+ .045	6/7 Dec.'55	H_9	- .148
70 sec.	H_δ	- .250*	9 min.	H_8	+ .128
	λ3729	- .265*		λ3869	+ .135
	λ3726	- .035		H_ϵ	+ .180
				H_δ	+ .310*
xf 896	λ4959	+ .260			
6/7 Dec.'55	H_β	+ .310	xf 898	λ3726	+ .310
3 min.	H_γ	+ .273	6/7 Dec.'55	λ3729	+ .120
	H_δ	+ .120	5 min.	λ3869	- .109
	H_ϵ	- .080		H_8	- .092
	H_8	- .148		H_ϵ	.000
	λ3869	- .170		H_δ	+ .216
	λ3726	+ .250			
	λ3729	+ .077			

Table 2.2. Nebular Emission Lines on IIa-J Plates (continued)

Plate, Date, Exposure	Line or Background of Line	$\log_{10} R(\lambda,t)$	Plate, Date, Exposure	Line or Background of Line	$\log_{10} R(\lambda,t)$
		Position E'			
xf 899	λ 3726	- .080	xf 901	H_{13}	- .220
6/7 Dec.'55	λ 3729	- .280	6/7 Dec.'55	H_{12}	- .200
70 sec.	H_δ	- .167	25 min.	H_{11}	- .108
	H_γ	+ .057		H_{10}	- .036
	H_β	+ .058		H_9	+ .078
	λ 4959	+ .013		H_8	+ .369
				λ 3869	+ .380
xf 900	H_β	+ .335		λ 4027	- .170
6/7 Dec.'55	H_δ	+ .200		λ 4471	+ .090
5 min.	H_ϵ	- .017	xf 902	H_{13}	- .036
	H_8	- .071	6/7 Dec.'55	H_{12}	+ .025
	λ 3869	- .077		H_{11}	+ .078
	λ 3729	+ .125		H_{10}	+ .170
	λ 3726	+ .330		H_9	+ .300
				λ 4027	+ .083
				b(4027)	- .313
				λ 4363	- .015
				b(4363)	- .280
				λ 4471	+ .340
				b(4471)	- .330

Table 2.2. Nebular Emission Lines on IIa-J Plates (continued)

Plate, Date, Exposure	Line or Background of Line	$\log_{10} R(\lambda,t)$	Plate, Date, Exposure	Line or Background of Line	$\log_{10} R(\lambda,t)$
		Position E'			
xf 1092	λ4959	+ .042	xf 1094	λ4471	- .257
7/8 Jan.'56	H_β	+ .130	7/8 Jan.'56	H_δ	+ .500
70 sec.	H_γ	+ .135	9 min.	λ4363	- .405*
	H_δ	- .182		H_ϵ	+ .200*
	λ3727	- .022		H_8	+ .130
	λ3729	- .254		λ3869	+ .108
				H_9	- .240
xf 1093	λ4959	+ .354		H_{10}	- .330
7/8 Jan.'56	H_β	+ .422		λ3726	+ .610*
3 min.	H_γ	+ .380		λ3729	+ .330
	H_δ	+ .077			
	H_ϵ	- .152	xf 1095	H_{13}	- .305
	H_8	- .278	7/8 Jan.'56	H_{12}	- .217
	λ3869	- .285	25 min.	H_{11}	- .138
	λ3727	+ .245		H_{10}	- .042
	λ3729	+ .035		H_9	+ .090
				λ3869	+ .480*
				H_8	+ .470*
				λ4027	- .210
				λ4363	- .260
				λ4471	+ .134

Table 2.2. Nebular Emission Lines on IIa-J Plates (continued)

Plate, Date, Exposure	Line or Background of Line	Log_{10} R(λ,t)	Plate, Date, Exposure	Line or Background of Line	Log_{10} R(λ,t)
		Position E'			
xf 1096	H_{13}	+ .085			
7/8 Jan.'56	H_{12}	+ .135			
75 min.	H_{11}	+ .213			
	H_{10}	+ .320			
	H_9	+ .467*			
	λ 4027	+ .203			
	b(4027)	- .253			
	λ 4363	+ .120			
	b(4363)	- .235			
	λ 4471	+ .482*			
	b(4471)	- .305			

Table 2.3. Reduction of a Typical Series of Spectrograms

Notation: $y = \mathrm{Log}_{10} \frac{f(t_1)}{f(t_2)}$ $\qquad \sigma = 0.67 \left(\sum_i \frac{(y_i - \bar{y})^2}{n(n-1)} \right)^{1/2}$

Plates	Exposure Times	$\bar{y}$	$\lvert y - \bar{y} \rvert_{ave.}$	Number Connecting Lines	σ
xf 926, 927	80^M, 23^M	.244	.029	6	.0045
xf 927, 928	23^M, 9^M	.371	.006	2	.0055
xf 928, 929	9^M, 3^M	.361	.030	4	.017
xf 929, 930	3^M, 70^S	.269	.018	4	.0085

real meaning. One source of systematic error is the dependence of reciprocity failure on wavelength. However, there was no obvious tendency for the quantities $R(t, \lambda)$ to vary with wavelength.

The ratios of $A(\lambda)\, E(\lambda)$ for any two lines follow directly from equation 2.11. For the lines $\lambda 4027$, $\lambda 4363$, and $\lambda 4471$ the background contributed a significant fraction of the total line strength and was taken into account in computing the line strengths. A display of the results will be deferred until after a discussion of the determination of $A(\lambda)$ from the comparison star plates.

The principal difficulty in the reduction of the comparison star tracings lay in the corrections for the absorption lines in the solar spectrum. It is clear that the instrumental resolving power affects the blackening on the plate at a given wavelength because of the blending of nearby absorption lines.

One method used to account for the lines was to inspect the Utrecht Photometric Atlas of the Solar Spectrum [19] and select regions which were near the lines of interest but which had a fairly constant and rather small fraction of the energy removed by lines. If such regions cover several times the resolving power of the optical system, the central portions of the regions should be unaffected by nearby strong lines. The flux of energy in the continuum was taken from data given by Minnaert [20], who lists values of the intensity at the center of the solar disc and of the ratio of the flux to the central intensity. These values are

the averages of several measurements by various authors. The flux of the continuum was corrected by the fraction of energy removed by the lines, as obtained from planimetry of the Photometric Atlas of the Solar Spectrum. This procedure is open to objection. Values of the continuous flux are obtained by assuming the continuum passes through the regions of the spectrum between lines, where the flux is greatest. The value which the flux between the absorption lines reaches depends on the resolving power of the optical equipment. The instruments on which the values of the continuous flux given by Minnaert were measured had much lower resolving power than those used to prepare the Utrecht atlas. Therefore, the continuum was probably believed by the intensity distribution observers to be lower than it is shown in the atlas. Hence use of the atlas probably overcorrects for absorption lines.

Two determinations of the energy curve of the sun by Pettit [21] and H.H. Plaskett [22] were also used for comparison with the values obtained by use of the atlas. These measurements included the effects of the solar lines. The dispersion used by Plaskett was about twice that used on the comparison spectra, and Pettit used a band of one hundred Angstroms in his measurements. The results of the three ways of finding the $E(\lambda)$ for the selected regions are given in Table 2.4.

The results of Pettit are not applicable in the blue regions where there are many strong absorption lines within one hundred Angstroms. For the comparison of $E(\lambda 4833)$ and $E(\lambda 5876)$, Pettit's measurement should be as valid as Plaskett's.

Table 2.4. Relative Solar Energy Fluxes

$\lambda_o \equiv 4838$ A.

	Utrecht Atlas		Pettit	Plaskett	Adopted
λ(Å)	% Absorbed by Lines	$\text{Log}_{10} \frac{E(\lambda)}{E(\lambda_o)}$	$\text{Log}_{10} \frac{E(\lambda)}{E(\lambda_o)}$	$\text{Log}_{10} \frac{E(\lambda)}{E(\lambda_o)}$	$\text{Log}_{10} \frac{E(\lambda)}{E(\lambda_o)}$
4011-4027	21.2	-0.072	- .099	- .050	- .055
4079-4091	19.4	- .063	- .104	- .052	- .055
4357-4368	17.8	- .047	- .046	- .035	- .039
4503-4520	7.5	+ .006	0.000	+ .015	+ .010
4832-4849	7.2	0.000	0.000	0.000	0.000
4962-4969	8.1	- .012	- .014	- .015	- .014
5360-5375	2.0	- .053	- .053	- .079	- .060

Note that Plaskett's values show that the use of the Utrecht atlas probably did slightly overcompensate for the lines.

The observational material for the solar energy distribution consisted of five plates in the blue spectral region. The pertinent observational data and important results for the five plates are given in Table 2.6.

The values of the adopted relative flux, given in Table 2.4, give values of $A(\lambda)$ by an application of equation 2.9. Table 2.5 lists the results.

Table 2.5. Sensitivity of IIa-J Emulsion

(Log_{10} $A(\lambda 4340) \equiv 1.$)

λ (Å)	Log_{10} $A(\lambda)$	λ (Å)	Log_{10} $A(\lambda)$
4015	+ .124	4511	+ .158
4085	+ .145	4840	0.000
4362	+ .203	4965	- .104

The determination of the relative values of $A(\lambda)$ for the various lines of interest necessitates some interpolation between the values of $A(\lambda)$ for the wavelengths which were convenient to use in the reduction of the solar spectrum. The final values of $A(\lambda)$ adopted are given in Table 2.7.

With the quantities $A(\lambda)$ and $E(\lambda)$ $A(\lambda)$ known, the intensities of the nebular lines relative to each other can be determined for each series of plates. These line strengths

Table 2.6. Summary of Data from IIa-J Comparison Plates

Plate	xf 780	xf 1022	xf 1077	xf 1081	xf 1082		
Star	85 Peg	HR 3750	HD 10307	HD 10307	HD 10307		
Mag.	5.75	5.44	4.94	4.94	4.94		
Exposure (seconds)	182	240	75	60	90		
Date	14/15 Nov. 1955	1/2 Jan. 1956	6/7 Jan. 1956	6/7 Jan. 1956	6/7 Jan. 1956		
λ(Å)	Y (λ)					Average	Average Deviation
4015	+ .075	+ .059	+ .042	+ .073	+ .092	+ .069	.013
4085	+ .070	+ .116	+ .085	+ .058	+ .122	+ .090	.023
4362	+ .180	+ .164	+ .187	+ .155	+ .125	+ .164	.019
4511	+ .147	+ .189	+ .200	+ .165	+ .140	+ .168	.021
4840	0.000	0.000	0.000	0.000	0.000	0.000	0.000
4965	- .128	- .108	- .128	- .100	- .115	- .118	.010

Notation: $Y(\lambda) = \log_{10} \frac{A(\lambda)\, E(\lambda)}{A(\lambda 4840)\, E(\lambda 4840)}$

All of the above plates taken with slit 8.0 mm. x .320 mm.

Table 2.7. Plate Sensitivity Factors

$A(\lambda 4840)\ E(\lambda 4840) \equiv 1.$

Line		$\log_{10} A(\lambda)$	Line		$\log_{10} A(\lambda)$
H_ϵ	$\lambda 3968$	+ .115	He I	$\lambda 4471$	+ .150
He I	$\lambda 4027$	+ .125	H_β	$\lambda 4861$	- .017
H_δ	$\lambda 4101$	+ .150	[O III]	$\lambda 4957$	- .082
[O III]	$\lambda 4363$	+ .203	[O III]	$\lambda 5007$	- .110
H_γ	$\lambda 4340$	+ .210	He I	$\lambda 5876$	+ .399

are given in Table 2.8. They must later be corrected for the reddening effects of absorption by dust.

The errors in the ratios of lines as given in Table 2.8 are indicated to some extent by the spread in the values of both $A(\lambda)\ E(\lambda)$, obtained from the nebular plates, and $A(\lambda)$, determined by the comparison star plates. These internal inconsistencies will indicate the magnitudes of random errors and the differences in systematic errors from night to night. The estimated error in $\log_{10} E(\lambda)$ was taken to be the square root of the sum of the squares of the average deviations of $\log_{10} A(\lambda)\ E(\lambda)$ and $\log_{10} A(\lambda)$. It is given in Table 2.9. This particular estimate of the error cannot be justified quantitatively. However, the results of probability theory are not directly applicable to results affected by nonrandom errors, such as the decisions of the author to weight a ratio $R(t, \lambda)$ by one, one-half, or zero in the averages to find $f(t_1)/f(t_2)$.

Table 2.8. Observed Line Intensities from IIa-J Plates

Quantities marked (*) are given half weight in averages.

$$\frac{[\lambda_1]}{[\lambda_2]} = \text{Log}_{10}\ \frac{E(\lambda_1)}{E(\lambda_2)}$$

Date of Series	$\frac{[3726]}{[3729]}$	$\frac{[H_\epsilon]}{[4027]}$	$\frac{[H_\delta]}{[4027]}$	$\frac{[H_\gamma]}{[4471]}$	$\frac{[4959]}{[4363]}$	$\frac{[5007]}{[4959]}$	$\frac{[H_\beta]}{[H_\gamma]}$	$\frac{[H_\beta]}{[H_\delta]}$	$\frac{[H_\beta]}{[H_\epsilon]}$
				Position B'					
7/8 Dec	-	.814*	1.070*	.788*	1.464*	.435	.039	.298	.554*
9/10 Dec.	.168	.872	1.106	1.009	1.532	.458	-.037	.260	.494
7/8 Jan.	.273	.822	1.052	.995	1.537	-	.010	.313	.543
8/9 Jan.	.242	.854	1.032	.872	1.649*	-	-	.330*	.508*
Average	.239	.845	1.064	.934	1.543	.447	.013	.296	.520
Average Deviation	.037	.022	.025	.077	.036	.012	.026	.021	.023
$\text{Log}_{10}\ \frac{A(\lambda_1)}{A(\lambda_2)}$	.000	.010	-.025	-.060	.285	.028	.227	.167	.132
$\text{Log}_{10}\ \frac{E(\lambda_1)}{E(\lambda_2)}$	.239	.855	1.039	.876	1.823	.475	.240	.463	.652
Estimated Error in Log	.037	.025	.039	.080	.047	.030	.033	.040	.038
Estimated Error	9°/o	6°/o	9°/o	20°/o	11°/o	7°/o	8°/o	10°/o	9°/o

Table 2.8. Observed Line Intensities from IIa-J Plate (continued)

Quantities marked (*) are given half weight in averages.

$$\frac{[\lambda_1]}{[\lambda_2]} = \text{Log}_{10}\ \frac{E(\lambda_1)}{E(\lambda_2)}$$

Date of Series	$\frac{[3726]}{[3729]}$	$\frac{[H_\epsilon]}{[4027]}$	$\frac{[H_\delta]}{[4027]}$	$\frac{[H_\gamma]}{[4471]}$	$\frac{[4959]}{[4363]}$	$\frac{[H_\beta]}{[H_\gamma]}$	$\frac{[H_\beta]}{[H_\delta]}$	$\frac{[H_\beta]}{[H_\epsilon]}$
				Position E'				
11/12 Nov.	.232	.849	1.149	.928	1.434	-.013	.166	.466
11/12 Nov.	.235	.785	1.056	.913	1.548	-.005	.212	.483
6/7 Dec.	.200	.815	1.053	.900	1.428*	-.019	.213	.448
7/8 Jan.	.276	.943	1.201	1.083	.1567	.018	.320	.578
Average	.236	.853	1.115	.959	1.513	-.004	.266	.497
Average Deviation	.026	.055	.060	.075	.048	.013	.035	.051
$\text{Log}_{10}\ \frac{A(\lambda_1)}{A(\lambda_2)}$	.000	.010	-.025	-.060	.285	.227	.167	.132
$\text{Log}_{10}\ \frac{E(\lambda_1)}{E(\lambda_2)}$	.236	.863	1.090	.899	1.798	.223	.433	.629
Estimated Error in Log	.026	.059	.064	.077	.058	.032	.045	.065
Estimated Error	6%	14%	16%	19%	14%	8%	11%	16%

Occasionally the inclusion of a line given half-weight affected the average materially. It was merely the opinion of the author that the inclusion of the line improved the value of the average, even though the blackening did correspond to a point off the characteristic curve.

The estimated errors of the observed line intensities are seen from Table 2.8 to be of the order of ten to twenty per cent. This should be a rather generous estimate of the random errors affecting the results.

Systematic errors which do not vary with time will not be reflected in internal inconsistencies. One such error lies in the estimation of the values of the emulsion sensitivity parameters $A(\lambda)$ for the wavelengths of the nebular lines from the values of $A(\lambda)$ at the line-free portions of the solar energy distribution. The value of $A(\lambda)$ for the lines of the shortest wavelength are possibly uncertain by ten per cent. It was felt that the inclusion of points in regions of heavy line absorption would probably lead to even worse errors, so no points of shorter wavelength than H_ϵ were added.

One check of the validity of the photometry was made; two plates of twenty-five seconds' exposure were made on the position B' in order to obtain both [OIII] λ4957 and λ5007 in measurable strength. The intensity ratio obtained from the two plates was $E(\lambda5007)/E(\lambda4957) = 2.98$, which is in very good agreement with the measured value of 3.00 and the theoretical value of 2.93 [23]. It should be noted that the ratio did not

involve comparison of lines on different plates, or significant corrections for plate sensitivity and differences in solar energy flux. Hence the ratio was really primarily a test of the correctness of the tracing and reduction procedures.

The reduction of the red plates simply involved the measurement of two lines on each plate, He I λ5876 and H_β. The treatment of the comparison star plates was equally simple, and there was comparatively little difficulty in correcting for the few absorption lines. The data which may be of interest for the comparison plates are given in Table 2.9. The data from the nebular plates are in Table 2.10. Note that the final intensity ratio $E(\lambda 5876)/E(H_\beta)$ is given at the bottom of Table 2.10.

Table 2.9. Reduction of Comparison Star Plates in Red

Star: HD 10307
Date: 4/5 Jan. 1956
Slit size: 8.0 mm x .320 mm.

Plate	Exposure (seconds)	$\text{Log}_{10} \frac{A(\lambda 5868)}{A(\lambda 4840)} \frac{E(\lambda 5868)}{E(\lambda 4840)}$
xf 1033	135	+ 0.390
xf 1035	120	+ 0.335
xf 1036	90	+ 0.325
xf 1037	75	+ 0.323
xf 1050	90	+ 0.323

Average: + 0.339
Average Deviation: .020

Log_{10} $E(\lambda 5876)/E(\lambda 4840)$: - .060
Log_{10} $A(\lambda 5876)/A(\lambda 4840)$: + .399

Table 2.10. Reduction of Nebular 103a-F(3) Plates
All plates with slit size 12 mm. x .800 mm.
Wratten #3 filter in optical system.
Quantities marked (*) given half weight in average.

Plate	Date (1956)	Position Exposure	$\text{Log}_{10} \frac{A(\lambda 5876)\ E(\lambda 5876)}{A(H_\beta)\ E(H_\beta)}$	
			B'	E'
xf 1003	1/2 Jan	B', 4 min.	- .350	
xf 1005	"	B', 4 min.	- .299	
xf 1054	5/6 Jan	B', 5 min.	- .382	
xf 1055	"	B', 7 min.	- .400*	
xf 1057	"	E', 6 min.		- .315
xf 1058	"	B', 6 min.	- .335	
xf 1060	"	B', $3\frac{1}{2}$ min.		- .375
		Average:	- .348	- .345
		Average Deviation:	.028	.030
		$\text{Log}_{10}\ A(\lambda 5876)/A(H_\beta)$:	+ .399	+ .399
		$\text{Log}_{10}\ E(\lambda 5876)/E(H_\beta)$:	- .747	- .744
		Estimated Error in Log:	.036	.036
		Estimated Error:	9%	9%

The line intensity ratios listed in Tables 2.8 and 2.10 are the final products of the observational programs.

C. Corrections for Reddening.

It is well known that interstellar dust absorbs blue light preferentially over red. There is a great deal of dust in the region of the Orion Nebula, and consequently the light from the nebula will be reddened. In this section an estimate will be made of the amount of reddening suffered by the nebular lines.

An estimate of the reddening of the nebular light can be obtained from the colors of the four stars of the Trapezium, θ' Ori. Stebbins and Whitford [9] obtained six-color relative brightnesses of the group as a whole. If a realistic estimate of the unreddened energy distribution of the light from the group can be made, the reddening effects of the absorption can be determined.

The classifications [24] and magnitudes [25] of the stars in the Trapezium are known. For each Trapezium star, a relatively unreddened star of the same spectral class can be found for which six-color measurements exist. The effects of normal reddening [26] can be removed from the six-color measurements by adjustment of the color index C_1 of the star to fit the intrinsic color index [24] of the star's spectral type. Morgan, Code and Whitford [27] have published an extensive list of the color indices of early-type stars.

Perhaps an example of the method for finding the intrinsic color of a star would be useful. The brightest star in the Trapezium is of spectral type O6 [25]. A relatively unreddened O6 star for which six-color measures exist is HD 199579, which has a color index C_1 of -0.12 magnitudes [27]. Since the intrinsic color C_1 of an O6 star is -0.30 magnitudes [24], the color excess E_1 is 0.18 magnitudes. On the six-color system the excess $E_{[V-I]}$ is 6.3 E_1, or 1.13 magnitudes. If the reddening of HD 199579 follows the normal reddening law, we can account for it and find the unreddened colors of the star. The procedure is indicated in Table 2.11. In a similar manner the intrinsic colors

of each of the four stars in the Trapezium can be found.

Table 2.11. Corrections for Reddening in HD 199579

Measured C_1 = -0.12 mag.
Intrinsic C_1 = -0.30 mag.
E_1 = 0.18 mag.
$E_{[V-I]} = 6.3\ E_1 = 1.13$ mag.

	U	V	B	G	R	I
Measured color of HD 199579 (magnitudes)	-1.77	-0.84	-0.35	-0.03	+0.38	+0.86
Normal Reddening ($E_{[V-I]}$= 1.13)	+0.74	+0.46	+0.25	+0.04	-0.28	-0.67
Intrinsic color of HD 199579	-2.51	-1.30	-0.60	-0.07	+0.66	+1.53

The energy distribution of the whole Trapezium can be found by weighting the energy distributions of the individual stars according to the brightnesses of the stars at λ5550 as determined by Sharpless [25]. The reddening can be determined by comparison of the observed with the true energy distribution.

Table 2.12 summarizes the essential features of the procedure used to obtain the reddening of the Trapezium. The final reddening found is given near the end of the table. It is compared to the normal reddening on the same basis as Stebbins and Whitford [9] used when they came to the conclusion that the reddening in the Trapezium is abnormal. The reddening law as derived in the present paper gives an anomaly of the reddening

Table 2.12. Determination of Color of Reddening of Trapezium

star	$m_{(\lambda 5550)}$	Spec.	Slightly reddened star, same spec.	Comparison star C_1	Intrinsic C_1
θ^1 Ori A	6.75	B0.5	HD 184915	-0.14	-0.25
" B	7.96	B3	HD 120315	-0.23	-0.22
" C	5.14	O6	Hd 199579	-0.12	-0.30
" D	6.70	B0.5	HD 184915	-0.14	-0.25

Color λ	U 3530	V 4220	B 4880	G 5700	R 7190	I 10300
Intrinsic Color (magnitudes):						
O.6	-2.51	-1.30	-0.60	-0.07	+0.66	+1.53
B0.5	-2.06	-1.11	-0.48	-0.07	+0.55	+1.33
B3	-1.80	-1.12	-0.52	-0.06	+0.58	+1.28
Magnitudes:						
O6, m = 5.14	2.81	3.98	4.72	5.25	4.98	6.85
B0.5, m = 6.70	4.79	5.74	6.37	6.78	7.40	8.18
B0.5, m = 6.75	4.84	5.79	6.42	6.83	7.45	8.23
B3, m = 7.96	6.30	6.98	7.58	8.04	8.68	9.38
Fluxes, O6 = 1.00						
O6, m = 5.14	1.000	1.000	1.000	1.000	1.000	1.000
B0.5, m = 6.70	0.162	0.198	0.219	0.244	0.271	.293
B0.5, m = 6.75	0.154	0.189	0.209	0.234	0.258	.280
B3, m = 7.96	0.040	0.063	0.072	0.076	0.083	.097

Table 2.12. Determination of Color of Reddening of Trapezium (continued)

Color	U	V	B	G	R	I
Sum of Fluxes						
absolute:	1.356	1.450	1.500	1.554	1.612	1.670
magnitudes:	-0.33	-0.40	-0.44	-0.48	-0.52	-0.56
Unreddened 06:	-2.51	-1.30	-0.60	-0.07	+0.66	+1.53
Intrinsic Color θ^1 Ori:	-2.84	-1.70	-1.04	-0.55	+0.14	+0.97
Measured Color (mag):	-1.64	-0.74	-0.29	+0.02	+0.27	+0.56
Excess (mag):	+1.20	+0.96	+0.75	+0.57	+0.13	-0.41
[B+G+R] = 0:	+0.72	+0.48	+0.27	+0.09	-0.35	-0.89
[U-I] = 1.00:	+0.45	+0.30	+0.17	+0.06	-0.22	-0.55
Normal reddening:	0.45	+0.25	+0.11	-0.05	-0.27	-0.55
Difference:	0.00	+0.05	+0.06	+0.11	+0.05	0.00
Stebbins and Whitford [24]:	0.00	+0.07	+o.09	+0.14	+0.09	0.00

in the Trapezium which is about two-thirds of that found by Stebbins and Whitford. The latter investigators assumed that the mean spectral type of the Trapezium is B0, which is slightly too late; O9 would be better [25].

The entire reddening found for the Trapezium stars does not necessarily apply to the nebular light. It is known from studies of the radial velocity distribution in the nebula that only material which is expanding towards the sun is visible [30]; either the far side of the nebula is cut off from our view by obscuring material in the nebula or the density of gas falls off rapidly on the far side of the Trapezium. In any case, the Trapezium is behind most of the nebular material which we can see, and the effective path length for the nebular light may be less than that for starlight.

A simple model for the nebula will now be considered. Let the nebula be a slab of gas with a path length S along a line of sight to the earth. Suppose the Trapezium is near the surface of the slab away from the earth. Assume that all of the material in the line of sight lies in the ionized region of the nebula, and that the distribution of dust and gas is such that the ratio of the emissivity per unit volume j_ν to the absorption per unit volume k_ν is everywhere constant.

The equation of transfer in the nebula is

$$dI_\nu = +I_\nu k_\nu ds - j_\nu ds \quad , \tag{2.12}$$

where I_ν is the specific intensity of light at the frequency ν

and the path length s is measured along the line of sight. It is to be taken as zero at the front surface and increasing away from the earth. If we define the optical depth τ_ν by

$$\tau_\nu = k_\nu s, \tag{2.13}$$

equation (2.12) becomes

$$dI = I_\nu \, d\tau_\nu - \frac{j_\nu}{k_\nu} d\tau_\nu \quad . \tag{2.14}$$

The solution of equation 2.14 can be written down immediately as

$$I_\nu (0) = \frac{j_\nu}{k_\nu} (1 - e^{-T_\nu}), \tag{2.15}$$

where $T_\nu = k_\nu S$.

If there were no absorptions, the ratio of the nebular intensities at two frequences ν_1 and ν_2 would be j_{ν_1}/j_{ν_2}. With absorption, the ratio is

$$\frac{I_{\nu_1}}{I_{\nu_2}} = \frac{k_{\nu_1}}{k_{\nu_1}} \frac{j_{\nu_2}}{j_{\nu_2}} \cdot \frac{(1 - e^{-T_{\nu_1}})}{(1 - e^{-T_{\nu_2}})} \quad . \tag{2.16}$$

The color excess $E^{neb}_{[\nu_1 - \nu_2]}$ is the ratio of the intensities with and without absorption expressed in magnitudes, or

$$E^{neb}_{[\ -B]} = -2.5 \log_{10} \frac{(1 - e^{-T_{\nu_2}})}{(1 - e^{-T_{\nu_1}})} \cdot \frac{k_{\nu_1}}{k_{\nu_2}} \tag{2.17}$$

$$= -2.5 \log_{10} \frac{T_{\nu_1}}{T_{\nu_2}} \frac{(1 - e^{-T_{\nu_2}})}{(1 - e^{-T_{\nu_1}})} \quad . \tag{2.18}$$

The situation is different for the star shining through the nebula; the surface brightness of the nebula is negligible with respect to the star, and the starlight is simply absorbed by the dust along the path length. Let $I^*_\nu(\tau_\nu)$ be the intensity of

the starlight at optical depth τ_ν. Then

$$I^*_\nu(0) = I^*_\nu(T_\nu)\, e^{-T_\nu} . \qquad (2.19)$$

Since the fraction of light absorbed in each frequence is e^{-T_ν}, the excess is given by

$$E^*_{[\nu_1-\nu_2]} = 2.5 \log_{10} e^{-(\tau_{\nu_2}-\tau_{\nu_1})} . \qquad (2.20)$$

The frequency ν_1 in equations 2.18 and 2.20 will be associated with the wavelength $\lambda 4880$, and ν_2 with $\lambda 4220$, corresponding to the effective wavelengths of the colors B and V respectively of the six-color system. The measured excess $E^*_{[B-V]}$ is 0.25 magnitudes. The total absorption, taken to be zero at infinite wavelength, can be found by extrapolation of a plot of the color excess as a function of reciprocal wavelength to infinite wavelength. This was done for a reddening with an $E_{[B-V]}$ of 0.19 magnitudes [29]; the total absorption was 1.08 magnitudes for point B and 1.27 magnitudes for V. The Trapezium was found in Table 2.12 to have an $E_{[B-V]}$ of 0.21 magnitudes, for which the total absorption is 1.19 magnitudes at B and 1.40 magnitudes at V. Converting to optical depth, we have

$$T_B = 1.10 \qquad T_V = 1.29$$

The color excess of the nebula can now be computed by equation 2.18. The result is

$$E^{neb}_{[B-V]} = -2.5 \log_{10} \frac{T_B}{T_V} \frac{(1 - e^{-T_V})}{(1 - e^{-T_B})} = 0.083 \text{ mag.} \qquad (2.21)$$

Since the excess of the star is 0.21 magnitudes, the nebula is reddened only forty per cent as much as the star.

If the thickness of the nebula were infinite but the star remained fixed relative to the front surface of the nebula, the color excess of the nebula would approach the ratio of the absorption coefficients, or 0.853. This excess would be 0.17 magnitudes, or four-fifths that of the star.

The star θ^2 Orionis is about 2' from the Trapezium but is considerably less reddened, probably because it lies close to the front boundary of the nebula. Probably much of the reddening of θ^2 Ori occurs in a region of neutral hydrogen lying in front of the ionized region. Absorption in this material will affect the nebular and stellar light equally, therefore the nebula should be at least as reddened as θ^2 Ori.

The color index C_1 of θ^2 Ori is -0.16 magnitudes [24], while the intrinsic color of a star of its spectral type (09.5) is -0.26. Therefore θ^2 Ori has an excess E_1 of 0.10 magnitudes. The Trapezium has a C_1 of -.02 magnitudes and the mean spectral type of an 09 star, which has an intrinsic C_1 of -0.27 magnitudes. The ratio of the excesses of θ^2 Ori and θ^1 Ori is then 0.10/0.25, and θ^2 Ori is reddened about forty per cent as much as θ' Ori.

The simplified model for the nebula has indicated that the nebula might suffer considerably less absorption than the Trapezium stars. A somewhat arbitrary decision had to be made regarding the reddening adopted for the nebular light. A reddening of one-half that of θ' Ori was finally used. The

decision was based in part on the values obtained for the Balmer decrement, as will be seen later.

The relative reddening in the wavelengths of the various nebular lines was found by a plot of the observed reddening of θ^1 Ori against $1/\lambda$.

The relative absorption in the wavelengths of the nebular lines is given in Table 2.13. The final unreddened line intensity ratios are given in Table 2.14. The notation employed in the tables for the unreddened or intrinsic nebular line intensity is $E^i(\lambda)$, and the factor which the reddening introduces normalized to one at H_β is $r(\lambda)$.

Table 2.13. Reddening Factors $r(\lambda)$

$r(H_\beta) = 1$

Line	$\log_{10} r(\lambda)$	Line	$\log_{10} r(\lambda)$
λ5876	-0.051		
λ4959	- .006	H_γ	+0.031
H_β	0.000	H_δ	+ .046
λ4471	+ .021	λ4027	+ .049
λ4363	+ .028	H_ϵ	+ .055

Table 2.14. Intrinsic Line Intensity Ratios in Orion

λ_1/λ_2	$\text{Log}_{10}\frac{r(\lambda_1)}{r(\lambda_2)}$	$\text{Log}_{10}\frac{E'(\lambda_1)}{E'(\lambda_2)}$
$H_\epsilon/\lambda 4027$	+ .006	0.861
$H_\delta/\lambda 4027$	- .003	1.036
$H_\gamma/\lambda 4471$	+ .010	.886
$\lambda 4959/\lambda 4363$	- .034	1.789
H_β/H_γ	- .031	.209
H_β/H_δ	- .046	.417
H_β/H_ϵ	- .055	.597
$H_\beta/\lambda 5876$	+ .051	.798

The values found for the Balmer decrement are of particular interest, because theory [15] indicates that the decrement should be quite insensitive to electron temperature, and can therefore serve as a check on photometry. However, as will be seen in the next chapter, the tneory from which the actual values of the decrement were calculated is open to objections. A comparison of values of the Balmer decrement obtained in this and in other investigations [4,30] and the theoretical decrement is given in Table 2.15. The theoretical values are taken for a temperature of 10,000°K.

The last entry in Table 2.15 gives the Balmer decrement obtained from the present investigation if the reddening for the nebular lines were taken to be equal to that observed in θ' Ori.

It is seen that the additional absorption correction makes the Balmer decrement less steep than that indicated by the other considerations. This fact served as a partial justification of the use of only one-half of the reddening of θ' Ori.

Table 2.15. The Balmer Decrement

Observer	Reference	H_β/H_γ	H_β/H_δ	H_β/H_ϵ
Mathis	-	0.62	0.38	0.25
Greenstein	4	0.60	0.37	0.20
Plaskett	31	0.48	0.19	-
Theory	15	0.51	0.31	0.21
Mathis*	-	0.67	0.42	0.28

* Entire reddening of θ' Ori taken for nebula.

Chapter III. Determination of the Relative Helium Abundance

A. Fundamentals of Theory.

In order to obtain the relative abundances of hydrogen and helium from the strengths of their lines, one must know the ratio of the number of atoms in each level giving rise to an observed transition to the total number of atoms. In a system which is not in thermodynamic equilibrium, the ratios of level populations must be found by detailed computation. Such calculations have been performed in considerable detail for the case of hydrogen by Menzel and other members of the Harvard College Observatory [15]. Calculations have been performed by Goldberg [31] and Wellmann [32] for helium, with only a few of the lowest levels taken into account. More detailed calculations are performed in the present thesis.

In order to calculate the population of a level under steady-state conditions, we set the number of atoms entering a level per unit time equal to the number leaving it. Let i be a running index denoting the levels of the atom with energies lower than that of the reference level j and let ℓ denote those with higher energies. If the radiation field has an energy density u_{ij} at the frequency corresponding to the transition from j to i, the balance of the population of level j is given by

$$N_j\Big[\sum_i (a_{ji} + u_{ij} B_{ji}) + \sum_\ell u_{j\ell} B_{j\ell}\Big] = \sum_i N_i B_{ij} u_{ij} + \sum_\ell N_\ell (A_{\ell j} + u_{\ell j} B_{\ell j}), \qquad (3.1)$$

where N_j is the number of atoms per unit volume in the level j and A_{ji}, B_{ji}, and B_{ij} are the conventional notations for the Einstein coefficients. The left side of equation 3.1 represents the number of atoms per second leaving level j; the right side, the number entering the level j. The physical meanings of the terms on the right of equation 3.1 are as follows: the first represents radiative excitations upward from the level i; the second, spontaneous emissions from level ℓ downward; the third, the stimulated emissions from level ℓ to j. The meaning of the terms on the left is clear by comparison with the terms on the right.

The radiation field u will be assumed to be the Planck function for the stellar temperature T_s, diluted by a factor W. Then

$$u_{ij} = W \frac{8\pi h \nu_{ij}^3}{c^3} \frac{1}{\exp(h\nu_{ij}/hT_s) - 1} . \qquad (3.2)$$

For most frequencies W is the geometrical dilution factor, although for the Lyman lines of hydrogen the absorbing properties of the nebula affect it strongly. The geometrical factor is given by the fraction of the celestial sphere subtended by the disc of the star as viewed from the point under consideration in the nebula. If R is the distance of the star from the point and R_s the radius of the star, then

$$W = \frac{1}{4\pi} \frac{(\pi R_s^2)}{R^2} = \left(\frac{R_s}{2R}\right)^2 . \qquad (3.3)$$

For a point in the Orion Nebula which appears to be thirty seconds of arc from the exciting star θ' Ori C, R is at least 15,000 astronomical units = 2×10^{17} cm. If the radius of θ' Ori C is ten solar radii, or 7×10^{11} cm., W is given by

$$W \leq \left(\frac{R_o}{2R}\right)^2 = 4 \times 10^{-12} . \qquad (3.4)$$

We can therefore say that W is less than 10^{-12} in our future analysis. Over most of the path length it is one or two orders of magnitude smaller.

Since the radiation in the nebulae is exceedingly diluted, the effect of stimulated emissions on the level populations is always negligible. For many levels, all terms in the balance equation 3.1 which contain u_{ij} are negligible in comparison with those which do not, and equation 3.1 becomes

$$N_j \sum_i A_{ji} = \sum_l N_l A_{lj} \qquad (3.5)$$

From equation 3.5 we see that the population of such a level is determined solely by the populations of the levels higher than it.

If a level m is metastable, the Einstein coefficient A_{mi} is small for all i and the radiative excitations represented by the term $N_m \sum_l u_{ml} B_{ml}$ on the left side of equation 3.1 may not be negligible in comparison with the term $N_m \sum_i A_{mi}$. The probability of a transition downward via some improbable process has to be compared with the probability of a radiative excitation upwards. If the radiative excitation is dominant, we have

$$N_m \sum_l u_{ml} B_{ml} = \sum_l N_l A_{lm} \qquad (3.6)$$

for the metastable level population. The coefficient of N_m in equation 3.6 is of the order of W times the coefficient of the N_j in equation 3.5. Hence the population of the metastable level is of the order of W^{-1} times the ratio of the atomic factors in the equations. The atomic factors determine the equilibrium populations, so the ratio of the population of the level m to that of level j in the nebula is roughly W^{-1} times the equilibrium ratio.

The radiative transitions up from the metastable level m will contribute to the populations of the higher levels, so that the levels j to which the transitions occur have balance equations of the form

$$N_j \sum_i A_{ji} = \sum_l N_l A_{lj} + N_m u_{jm} B_{mj}. \qquad (3.7)$$

The population of a level is thus not determined by the populations of the higher levels alone if the level can undergo transitions to a level m from which radiative excitation is not negligible.

The computation of the populations of the various levels is simplified if we write the population N_j of the level j as

$$N_j = b_j N^+ Ne \frac{h}{(2\pi mkT_e)^{3/2}} \frac{g_j}{2g^+} e^{\Phi_i kT_e} \qquad (3.8)$$

where N^+ and Ne are the number of ions of the element and electrons per unit volume respectively, T_e is the electron temperature at the point considered, g_j and g^+ are the statistical weights, and h, m, and k are conventional notations for constants. The Φ_j is the ionization energy of the level. The

factor b_n is the ratio of the actual population of the level to the equilibrium population at temperature T_e. If $b_j = 1$, equation 3.8 becomes the standard Boltzmann-Saha equation.

The distribution function of the kinetic energies of the free electrons is the Maxwellian or equilibrium distribution for the temperature T_e. Let us consider the energies of the electrons as energy levels in the continuum of the atom. Then the parameter b_K of each such level is equal to unity. Since the relative populations of all levels in the continuum are known, quantities involving interactions of atoms with electrons of a given velocity range in the continuum can be expressed in terms of the total population of the continuum states. Therefore we will consider the continuum as one level of the atom in future discussions.

The correspondence principle of quantum mechanics requires the properties of the levels of the atom to merge with those of the continuum in the limit of high quantum numbers. The b values of very high levels will therefore be unity.

For the remainder of the chapter we will consider the triplet levels of helium explicitly. Before we can determine the populations of the higher triplet levels, we must know whether most of the transitions from the metastable 2^3S level are to the ground state or to the higher triplet levels. Transitions can occur to the ground state either by the simultaneous emission of two photons or by superelastic collisions with electrons. Excitations to higher levels can be either radiative or collisional. We will consider all of the above types of processes, starting with de-excitation by superelastic collisions.

B. The Electron Density and Superelastic Collisions.

The general expression for the probability P_{ij} per unit time that a helium atom in the level j will undergo a collision with an electron and make a transition to the state i (not necessarily lower in energy than j) is given by

$$P_{ij} = \int_o^\infty \frac{dN_e(v)}{dv} \quad \sigma_{ij}(v)\ v\ dv\ , \qquad (3.9)$$

where v is the velocity, dN_e/dv is the number of electrons with velocity in the range of velocities between v and v + dv per unit volume, and $\sigma_{ij}(v)$ is the cross-section for the process. Since the velocity distribution is Maxwellian, the only unknowns in equation 3.9 are the total number of electrons per volume and the function $\sigma_{ij}(v)$.

We will consider the electron density first. It can be estimated from the relative strengths of the [OII] lines λ3726, λ3729, which arise from transitions from the $^2D_{3/2}$ and $^2D_{5/2}$ states in [OII] to the ground $^4S_{3/2}$ state. The lines are excited by collisions of OII ions with electrons and de-excited by collisions undergone while in the excited states, and the intensity ratio therefore depends on the electron density. Seaton [33] has calculated the variation of the intensity ratio with density and temperature, and finds

$$\frac{E(\lambda 3729)}{E(\lambda 3726)} = 1.5\ \frac{1 + 2.26x}{1 + 10.0x}\ , \qquad (3.10)$$

where $x = 10^{-2}\ N_e\ T_e^{-1/2}$.

The ratio of the line strengths was determined observationally. Its logarithm as given by Table 2.8 of Chapter II is -0.239 for position B' and -0.236 for E'. Since the lines are at essentially the same wavelength, this value will not be modified by absorption. Substituting in equation 3.10, we get $x = 0.383$. For the value of T_e in equation 3.10 we will anticipate the results derived later in this chapter and use $10{,}000^{\circ}K$. We then get a value for the electron density of

$$N_e = 3.8 \times 10^3 \text{ cm.}^{-3} .$$

The probability of superelastic collisions de-exciting the atom from the 2^3S level to the 1^1S will now be considered. Determination of the cross-section is a difficult problem, but Massey and Moiseiwitsch [33] have computed an approximate cross-section for the inverse process of collisional excitation of the 2^3S level from the 1^1S level. Let the cross-section for this process be called σ_{12} and the one for superelastic collisions be called σ_{21}. Consideration of the principle of detailed balancing applied to a system in equilibrium results in the expression

$$\frac{\sigma_{21}}{\sigma_{12}} = \frac{g_1}{g_2} \frac{\epsilon + \Phi_{12}}{\epsilon} , \qquad (3.11)$$

where g's are statistical weights, ϵ is the energy the electron has before a superelastic collision, and Φ_{12} is the excitation energy of the 2^3S level.

The results of Massey and Moiseiwitsch were represented by a simple cubic polynomial so that an integration over the cross-section could be readily performed. The simplified relation

adopted was

$$\sigma_{12}(\epsilon) = 10^{-2}[2.6 + 10.5(1.6-\epsilon)^3]\pi a_o^2 \qquad (\epsilon \leq 1.6 \text{ e.v.})$$
$$= 2.6 \times 10^{-2}\ \pi a_o^2\ , \qquad (\epsilon \geq 1.6 \text{ e.v.}) \quad (3.12)$$

where a_o is the first Bohr radius. The energy ϵ is to be measured in electron volts and σ_{12} in square centimeters.

The quantities entering the expression for the probability P_{21} of superelastic collisions from 2^3S to 1^1S in helium have now been estimated, and P_{21} can be evaluated. Equation 3.8 becomes

$$P_{21} = \frac{1}{3}\frac{2\pi N_e}{(\pi kT_e)^{3/2}}\left(\frac{2}{m}\right)^{1/2}\int_o^\infty (\epsilon + 19.73)\,\sigma_{12}(\epsilon)\, e^{-\epsilon/kT_e}\, d\epsilon\ . \quad (3.13)$$

Substitution of the simplified form for $\sigma_{12}(\epsilon)$ as given by equation 3.13 gives

$$P_{21} = 1.9 \times 10^{-9}\ N_e = 7.1 \times 10^{-6}\ \text{sec.}^{-1}\ , \quad (3.14)$$

where the value of N_e found from the [O II] lines has been used.

The process of two-photon emission from the 2^3S level in helium is in competition with that of de-excitation by superelastic collisions. The probability per unit time P_{2Ph} of two-photon emission is derived at some length in Chapter IV and is found to be

$$P_{2Ph} = 1.1 \times 10^{-5}\ \text{sec.}^{-1} \quad (3.15)$$

Comparison of P_{21} and P_{2Ph} shows that collisions and two-photon emissions are competitive at the density found in the Orion Nebula. The total probability per unit time of a transition from the 2^3S to the 1^1S level in helium will be

$$P = P_{21} + P_{2Ph} = 1.8 \times 10^{-5} \text{ sec.}^{-1} \qquad (3.16)$$

A discussion of the possible effects of collisional excitations from the 2^3S level will be deferred until later. The populations of the triplet levels in helium will be determined on the assumption that the effects of collisional excitations are negligible. The assumption will be checked after the level populations have been computed.

C. Computations of Triplet Level Populations in Helium.

In principle the problem of determining the populations of the various triplet levels is a simple one; balance equations of the form of equation 3.1 can be written for as many levels as one chooses and the system of equations solved for the level populations. We will provisionally assume that collisional and radiative transitions are negligible even from the 2^3S level. Then the population of each level depends only on the populations of the levels above it with which radiative transitions can take place.

The actual solution of the system of balance equations is made easier if we introduce the oscillator strength f_{ij} in place of the Einstein coefficients. The appropriate relations are:

$$A_{ji} = \frac{8\pi^2 e^2 \nu_{ij}^2}{mc^3} \frac{g_i}{g_j} f_{ij} \qquad (3.17)$$

$$B_{ij} = \frac{g_i}{g_j} \frac{\pi e^2}{mh \nu_{ij}} f_{ij} \qquad (3.18)$$

$$B_{ji} = \frac{\pi e^2}{mh\,\nu_{ij}}\, f_{ij} \,. \tag{3.19}$$

Equation 3.1 becomes, if the definitions of b_j and the Einstein coefficients are substituted,

$$\sum_i b_i D_{ij} + \sum_\ell b_\ell D_{j\ell} = b_j D_{jj} \,, \tag{3.20}$$

where

$$D_{ij} = g_i f_{ij} \nu_{ij}^2 e^{\Phi_i/kT_e} \frac{W}{\left(e^{h\nu_{ij}/kT_s} - 1\right)} \,. \tag{3.21}$$

$$D_{ji} = g_i f_{ij} \nu_{ij}^2 e^{\Phi_j/kT_e} \left(1 + \frac{W}{e^{h\nu/kT_s} - 1}\right) \tag{3.22}$$

$$D_{jj} = \sum_i D_{ji} + \sum_\ell D_{j\ell} \tag{3.23}$$

In all of the above equations the convention is employed that states with a running index i lie lower in energy than state j, and those with ℓ lie higher.

In a dilute radiation field the second term in the parentheses in equation 3.22 is always negligible; it represents stimulated emissions. Except perhaps for the metastable 2^3S level, the D_{ij} terms in the definition of D_{jj} (equation 3.23) are also negligible. They correspond to radiative excitations. For the metastable 2^3S level they must be compared with the term representing de-excitations to the ground state.

Before numerical values of the various D_{ji} coefficients can be computed, the oscillator strengths f_{ji} must be known. Wellmann [33] has collected into a convenient table the results of computations of f values for helium by Go[illegible]g [34] and

Hylleraas [35]. For the higher levels of helium, the wave function of the excited electron becomes hydrogenic and the f values for hydrogen are applicable.

For the present investigations the f values were used as tabulated by Wellmann [3] between low states. Hydrogenic f values were computed from standard formulae [36,37] for transitions which Wellmann does not list. Tables of the hydrogenic f values are given in Appendix B.

For transitions from any level j to levels with very high quantum number n the f value asymptotically approaches the form

$$f_{jn} = \frac{\alpha_j}{n^3 \nu_{jn}^m} \quad , \tag{3.24}$$

where α_j is a constant depending on the level j and m is either two or three, depending on the level j. For the transitions from the 2^3S and 2^3P levels, Wellmann uses the values of the α_j computed by Goldberg [34]. For other levels Wellmann obtained estimates of α_j from values of the f values of the lower transitions. For levels with hydrogenic energies, which include all levels except 2S, 2P, 3S, 3P, and 4S, the hydrogenic α_j's are appropriate and differ sometimes by fifty per cent from Wellmann's, which therefore appear to be incorrect. The hydrogenic f values were used in the present investigation.

The asymptotic form of the f value for high quantum numbers can be used for states in the continuum. Let the energy of a given state p in the continuum be $Ry/\varkappa^2$, where Ry is the Rydberg number, in units of electron volts. Then for transitions

from the level j to the continuum we have

$$f_{jp} = \frac{\alpha_j}{\kappa^3 \nu_{jp}^m} \quad , \tag{3.25}$$

where all quantities have the same definitions as in equation 3.24. Conservation of energy requires that

$$h\nu_{jp} = \Phi_j + Ry/\kappa^2 \quad , \tag{3.26}$$

so

$$-d\kappa = \frac{h}{2Ry}\kappa^3 \, d\nu \quad . \tag{3.27}$$

If all of the levels in the continuum are considered as one level, designated by subscript K, we have

$$D_{jK} = W \frac{\alpha_j h}{2Ry} g_j e^{\Phi_j/kT_e} \int_{h\nu = \Phi_j}^{\infty} \frac{\nu^{2-m} d\nu}{e^{h\nu/kT_s} - 1} \tag{3.29}$$

$$D_{Kj} = \frac{\alpha_i h g_j}{2Ry} e^{\Phi_j/kT_e} \int_{h\nu = \Phi_j}^{\infty} \nu^{2-m} e^{-h\nu/kT_e} \, d\nu. \tag{3.30}$$

If we also wish to consider all levels with quantum numbers between n_i and n_f as one level L with the average properties of the levels in the interval, we write expressions similar to equation 3.29 and 3.30 with sums over the quantum number replacing the integral over the frequency.

The integrals occurring in equations 3.29 and 3.30 are easy to evaluate, and the expressions become

$$D_{jK} = \frac{1}{2} e^2 h^{-2} W \alpha_j g_j e^{\Phi_j/kT_e} kT_s (Ry)^{-1} \left[\ln\left(\frac{1}{e^{w_j} - 1}\right) + w_j\right] \tag{3.31}$$

for $m = 2$, where

$$w_j = \frac{\Phi_j}{kT_s} \tag{3.32}$$

The α_j in equation 3.31 and in all subsequent equations will be expressed in units such that the defining equation 3.24 holds when ν_{jm} is expressed in electron volts. The factors $e^2 h^{-2}$ on the right side of equation 3.31 arise from this choice of units. The energies (Ry) and kT will be considered to be expressed in electron volts.

Similarly,

$$D_{Kj} = \frac{1}{2} e^2 h^{-2} \alpha_j g_j (Ry)^{-1} kT_e \qquad (\text{for } m = 2) \tag{3.33}$$

$$D_{Kj} = -\frac{1}{2} e^2 h^{-2} \alpha_j g_j (Ry)^{-1} e^{\Phi_j/kT_e} Ei(-\Phi_j/kT_e)$$

$$(\text{for } m = 3) \tag{3.34}$$

where $-Ei(-x)$ is the exponential integral defined by

$$-Ei(-x) = \int_1^\infty e^{-ux} u^{-1} du \, . \tag{3.35}$$

In considering transitions to a level j from level L, representing the mean of all levels with quantum numbers above n_i, the sum over n can be approximated by an integral. Then

$$D_{ij} = \frac{1}{2} e^2 h^{-2} \alpha_j g_j kT_e (Ry)^{-1} (e^{Ry/kT_e(n_i - \frac{1}{2})^2} - 1)$$

$$(\text{for } m = 2) \tag{3.36}$$

$$D_{ij} = -\frac{1}{2} e^2 h^{-2} \alpha_j g_j (Ry)^{-1} e^{\Phi_j/kT_e} \left[Ei\left(-\frac{\Phi_j - (Ry)/(n_i - \frac{1}{2})}{kT_e}\right) - Ei\left(-\frac{i}{kT_e}\right) \right] \quad (\text{for } m = 3) \tag{3.37}$$

The helium line strengths observed in this investigation and the transitions involved were $\lambda 5876$, $2^3P - 3^3D$; $\lambda 4471$, $2^3P - 4^3D$; $\lambda 4027$, $2^3P - 5^3D$. Therefore only the populations of the 3^3D, 4^3D, and 5^3D levels in helium are needed to derive the relative strengths of the helium lines. The populations of the upper levels of the Balmer lines are needed in addition to derive the ratio of helium to hydrogen.

The populations of the ^3D levels of interest were found by explicit consideration of eighteen of the lowest triplet levels. The terms $\sum_{\ell} b_{\ell} D_{j\ell}$ on the left of equation 3.20 were taken approximately into account for levels up to $n = 30$ by using the results of Menzel [15] for hydrogen in a nebula which is optically thin in Lyman line radiation. Menzel gives only the mean value of b_n for all angular momentum states with a principal quantum number n; for the present paper, each degenerate angular momentum state was assumed to have Menzel's average b_n appropriate to the n of the state.

The coefficients D_{ji} can be written as

$$D_{ji} = d_{ji}\, e^{\Phi_j/kT_e}, \qquad (3.38)$$

where the entire dependence on the electron temperature is now in the factor e^{Φ_j/kT_e}. The coefficients d_{ji} can be tabulated once and for all, and are listed in Appendix C.

The coefficients D_{ij}, which represent radiative excitations from level i to j and are therefore proportional to W, were neglected except when i represented the 2^3S level. Collisional

excitations were neglected from all levels. With these assumptions the values of b_j were calculated in detail for an electron temperature of 10,000°K and a stellar temperature of 50,000°K for the eighteen levels listed in Table 3.1. The decay probability of the 2^3S level as found in the preceding section (equations 3.16) was used. The contributions of the levels for $n > 30$ were lumped into a level L and taken into account with the assumption that $b_L = 0.7$.

The value of D_{22}, which indicates the mode of transition from the 2^3S level, was found to be

$$D_{22} = 2.75 \times 10^{-8} + 2620\ W. \qquad (3.39)$$

We see that for $W < 10^{-11}$, the decays downward to the ground state dominate the radiative excitations. Since W is less than 10^{-12} in the nebula, the radiative excitations are certainly negligible. Our results are therefore independent of the unknown color temperature of the Trapezium beyond the Lyman limit.

The results of the computation are given in Table 3.1. The sixth column gives b'_j, or the value of b_j computed on the assumption that the contribution of the term $\sum_\ell b_\ell D_{j\ell}$ to all levels for ℓ up to thirty is larger by a factor of two. It is seen that b'_j differs from b_j by about twenty per cent for the ^3D levels of interest. This result indicates how influential the values of the b_ℓ for higher helium levels are on the results of the calculation. As will be seen, the use of Menzel's average b'_n s in the computation for the helium level populations might be in error by perhaps a factor of two.

The assumption that b_j is constant for different angular momenta with the same principal quantum number is shown in Table 3.1 to be very poor for low levels in helium, and is probably equally bad for high levels of both helium and hydrogen. The computed values for the Balmer decrement [15] therefore become suspect because of the wide variations of the b values between states of different L and the same n. If Menzel's values are an average of the b for the entire level, they represent mainly the b values of the higher L states with a given n. The Balmer lines can be produced only by atoms initially in a n^2S, P, or D state. Therefore it is somewhat dangerous to assume that the strengths of the Balmer lines can be computed from the average b_n for a level.

The values of b_j for T_e = 8,000°, 11,000°, and 12,000°K were computed with the radiative excitations of all levels neglected. The transitions from the level L, representing the high values of n, were small enough for T_e = 10,000°K to justify their neglect for other temperatures.

The values of the b_j found for the eighteen levels considered are given in Table 3.2 for the four temperatures considered. Values of b_j for temperatues in the range from 8,000° to 12,000° can be found by interpolation.

Table 3.1. Helium Levels Considered in Calculations

$T_e = 10{,}000^{\circ}K$

Level	j	Φ_j (e.v.)	$\sum_{\ell}' b_\ell D_{j\ell}$	b_j	b'_j
1^1S	1	24.58	-	-	-
2^3S	2	4.77	.541	1.5×10^9	1.9×10^9
2^3P	3	3.62	2.50	.21	.26
3^3S	4	1.87	.013	.030	.036
3^3P	5	1.58	.589	.29	.34
3^3D	6	1.51	.576	.079	.093
4^3S	7	0.993	.208	.058	.066
4^3P	8	0.879	.171	.23	.28
4^3D	9	0.851	.356	.11	.13
4^3F	10	0.850	.321	.20	.24
5^3P	11	0.559	.231	.55	.71
5^3D	12	0.545	.213	.11	.13
5^3F	13	0.544	.278	.29	.35
5^3G	14	0.544	.731	.23	.38
6^3D	15	0.376	.170	.11	.14
6^3F	16	0.376	.204	.31	.39
6^3G	17	0.376	.365	.37	.42
7^3F	18	0.277	.151	.34	.44
7^3G	19	0.277	.192	.44	.58

Table 3.2. The Coefficients b_j for Various Electron Temperatures

Level	j	T_e = 8000° b_j	T_e =10,000° b_j	T_e=11,000° b_j	T_e=12,000° b_j
2^3S	2	-	1.52×10^9	1.94×10^9	-
2^3P	3	.065	.214	.339	.576
3^3S	4	.015	.030	.038	.048
3^3P	5	.156	.290	.361	.442
3^3D	6	.044	.079	.098	.117
4^3S	7	.038	.058	.068	.078
4^3P	8	.155	.230	.267	.304
4^3D	9	.076	.111	.128	.144
4^3D	10	.137	.198	.228	.258
5^3P	11	.411	.550	.613	.674
5^3D	12	.083	.112	.124	.136
5^3F	13	.218	.289	.322	.355
5^3G	14	.176	.230	.260	.284
6^3D	15	.085	.114	.128	.138
6^3F	16	.248	.312	.341	.368
6^3G	17	.297	.372	.406	.440
7^3F	18	.223	.310	.334	.360
7^3G	19	.336	.444	.479	.510

D. The Ratio of Helium to Hydrogen.

The ratio of abundances of helium to hydrogen can be easily determined if the values of the b_j parameters for the upper levels of the observed lines can be found. Since the parameters depend on the electron temperature, the average value of T_e along the line of sight in the slit positions must be determined.

This temperature can be determined from the relative strengths of [OIII] lines. One of these lines, $\lambda 4363$, arises from a level of higher excitation than the level from which the other two, $\lambda 4959$ and $\lambda 5007$, arise. The ratio of the strengths of these lines depends on the temperature T_e. The detailed theory of this relation has been discussed by Seaton [17]. The expression which relates the ratio of the lines and the electron temperature is

$$\frac{E(\lambda 4959) + E(\lambda 5007)}{E(\lambda 4363)} = 8.74\ e^{3.30/t}, \qquad (3.39)$$

where $t = 10^{-4}\ T_e$. For the observed nebular lines, the ratio $E(\lambda 4959)/E(\lambda 4363)$ corrected for reddening, is 61.5 for position B' and 62.8 for position E'. If the ratio $E(\lambda 5007)/E(\lambda 4959)$ is taken as 2.95, a mean of the observed and theoretical values, the left side of equation 3.39 becomes 243 for B' and 248 for E'. Then

$$T_e = 9{,}900^{\circ}K \quad \text{(for E')}$$
$$T_e = 10{,}000^{\circ}K \quad \text{(for B')}\ . \qquad (3.40)$$

The coefficient of the exponential in equation 3.39 may, according to Seaton's estimate, be forty per cent in error, which would introduce a ten per cent error in T_e. The photometry should

have an error of less than twenty per cent. We will consider the value of T_e to be uncertain within ten per cent.

With the electron temperature known, the values of the quantities b_j for helium can be interpolated from the results given in Table 3.2. The values of b_n for the hydrogen levels were taken from Menzel and Baker's calculations [38] based on the assumption that the nebula is opaque to Lyman line radiation, called by Menzel Case B. The results are given in Table 3.3.

Table 3.3. Values of b_j Pertaining to Nebular Lines of Interest

Element	Level	Position E' b_j	Position B' b_j
He	3^3D	.078	.079
He	4^3D	.110	.111
He	5^3D	.111	.112
H	$4^2S,P,D$	.163	.166
H	$5^2S,P,D$	.229	.233
H	$6^2S,P,D$	.292	.296
H	$7^2S,P,D$	.337	.341

The intensity $I(\lambda)$ of the radiation which arises from a transition from the upper level j to the lower level i (where i represents 2^3P for helium and $2^2S,P$ for hydrogen) is

$$I(\lambda) = N_j A_{ji} h \nu_{ij} . \qquad (3.41)$$

From the definition of the A_{ji} in terms of f_{ij} (equation 3.17) and the defining equation for b_j (equation 3.8), the ratio of the intensities of a helium line to a hydrogen line becomes

$$\frac{I(\lambda)_{He}}{I(\lambda)_{H}} = \frac{b_{j(He)} \cdot N^{+}_{(He)} \cdot e^{\Phi_j/kT_e} \cdot \nu_{jk}^{3} \cdot g_{k(He)} f_{kj(He)}}{2b_{i(H)} \quad N^{+}_{(H)} \; e^{\Phi_i/kT_e} \cdot \nu_{im}^{3} \cdot g_{m(H)} f_{mi(H)}}, \qquad (3.42)$$

where j represents the upper level of the helium transition, k the lower helium level, i the upper hydrogen level, and m the lower hydrogen level.

All quantities are known in equation 3.42 except the ratio of the numbers of helium and hydrogen ions per unit volume. Since almost all of the atoms of both elements are ionized in the nebula, and the path lengths of the line emission of both elements are the same, the abundance ratio of the atoms is equal to the ratio of the numbers of ions per unit volume.

With the values of the quantities b taken from Table 3.3 and the f values for hydrogen from Menzel and Pekeris[39], the final results for the ratio of helium to hydrogen can be obtained. The results are tabulated in Table 3.4.

A source of error other than the photometry lies in the fact that b_j for the lowest D state is influenced more than the higher ones by transitions which have not been taken into account explicitly. Most of the transitions into the 3^3D level come from 4^3F, which in turn is strongly influenced by 5^3G, and so on.

Table 3.4. The Relative Abundance of Helium in the Orion Nebula

Line Ratio Used	Position E' Abundance By Number	Position E' Abundance By Mass	Position B' Abundance By Number	Position B' Abundance By Mass
$\lambda 4027/H_\epsilon$	.141	.36	.142	.36
$\lambda 4027/H_\delta$	.145	.37	.146	.37
$\lambda 4471/H_\gamma$	.133	.35	.134	.35
$\lambda 5876/H_\beta$	.105	.30	.106	.30
Average	.128	.34	.128	.34
Average Deviation	.015	.02	.015	.02

Most of the atoms in the high n levels are in the high L states, and the most probable transition from a state with numbers n and L is to the state with angular momentum of quantum number L-1 and the lowest possible principal quantum number. Once the atom is in a level with the highest possible L, it must remain in the highest L state for all of its subsequent cascading. Therefore it will eventually make a transition from the 4^3F into the 3^3D state. The higher ^3D states are hardly influenced by the transitions occurring at high n and L.

One way to test the consistency of the calculation of the b_j values for the helium lines is to compare the predicted line strengths of the helium lines themselves, which would eliminate reliance on the use of Menzel's b values for any specific state in hydrogen. The ratios depend only on the electron temperature and the b_j values. The results of the calculations are that the

ratio of $E(\lambda 4027)/E(\lambda 4471)$ should be 0.386 on the basis of the calculated b_j's and was observed to be 0.432, which is a difference of 11.2% of the average. The ratio $E(\lambda 4471)/E(\lambda 5876)$ should be 0.346 theoretically and was 0.278 observationally. The difference in this case is 21.8% of the average. The fact that the theoretical $E(\lambda 4471)/E(\lambda 5876)$ is predicted too high by 20% indicates that the b_{3D} is probably somewhat too low. Increasing b_{3D} would make the helium abundance obtained by comparison with H_β be more in line with that obtained from the other two lines.

It is hardly surprising that observational checks of the theory show discrepancies of ten to twenty per cent, since the approximations involved in the theory and the inherent errors of photometry introduce errors of about that size.

It is also possible that the value of b for hydrogen is fifteen per cent lower relative to the average b value of the S, P, and D states than are the b values for the other Balmer lines. If this were true, the observed Balmer decrement would be exactly the predicted one and the helium determinations of all helium lines would agree well. One would expect the average value of b_n to be closest to the b_n appropriate to Balmer transitions for low values of n. For this explanation to be correct, the average b for the S, P, and D states would have to bear constant ratios to the b_n's for the entire level for the higher levels, since the observed Balmer decrement for H_γ, H_δ, and H_ϵ was exactly as predicted by theory. Detailed calculations of the b values for the various angular momenta for hydrogen would be most helpful.

With the population of the 2^3S level relative to the higher triplet levels at our disposal, we can see if the collisional excitations from the level are indeed negligible, as was assumed in the calculations. The criterion will be that the number of atoms entering the state by radiative cascading should be much greater than the number entering by collisions. Since the numbers entering and leaving were equal in our model for calculations, we will compute the number leaving the level per unit time for convenience.

The number of excitations per unit time from the 2^3S level to the 2^3P is

$$\left(\frac{dN}{dt}\right)_{coll.} = N_{2S} \cdot \sigma \int_{\Phi_{21}}^{\infty} \frac{dN}{dv} \cdot v \; dv = N_{2S} \cdot \sigma \cdot 8.21 \times 10^8 \text{ sec.}^{-1} \tag{3.43}$$

The number leaving the 2^3P is

$$-\left(\frac{dN}{dt}\right)_{rad} = N_{2P}/\tau = 10^7 \, N_{2P} \text{ sec.}^{-1} , \tag{3.44}$$

where τ is the mean lifetime in the 2^3P level. The ratio of the excitations to the number leaving, is

$$\left(\frac{dN}{dt}\right)_{coll.} \Big/ \left(\frac{dN}{dt}\right)_{rad} = \frac{N_{2S} \cdot \sigma \cdot 8.2 \times 10^8}{N_{2P} \; 10^7}$$

$$= 1.97 \times 10^{14} \sigma \; . \tag{3.45}$$

Thus for any reasonable value of σ the ratio is very small indeed, and collisional excitations are negligible. This result justifies the basis upon which the b values were computed.

E. Absorption of $\lambda 3889$ in the Orion Nebula.

A strong absoprtion line of He I at $\lambda 3889$, arising from a $2^3S - 3^3P$ transition, was observed by O.C. Wilson. He found that the line has an equivalent width of 0.20 Angstroms in θ' Ori C. In this section the relation of the line strength to the path length of the nebula in front of the star will be considered.

The minimum path length will be found by equating the strength of the absorption line to the number of atoms capable of absorbing the line times the absorption coefficient per atom. Then the equivalent width W is given by

$$W = N_2 \, L \, \lambda^2 \frac{\pi e^2}{mc^2} f_{25}, \qquad (3.46)$$

where N_2 is the number of atoms of helium in the 2^3S state per unit volume, f_{25} is the oscillator strength of the $2^3S - 3^3P$ transition, and L is the path length in the ionized nebula between the earth and the star.

The quantity N_2 can be determined from equation 3.8, given the values of b_2 found for a temperature of 10,000°K, the electron density, and the abundance ratio of helium and hydrogen. We assume that all electrons are contributed by either helium or hydrogen. Then

$$N_2 = b_2 \frac{x}{1+x} \, N_e^2 \frac{h^3}{(2\, mkT_e)^{3/2}} \, \frac{3}{4} \, e^{\Phi_2/kT_e}, \qquad (3.47)$$

where $x = \frac{N_{He}}{N_H} = .139$. Substitution of the various quantities appearing in equation 3.47 gives

$$N_2 = 2.4 \times 10^{-4} \text{ cm.}^{-3} \qquad (3.48)$$

If equation 3.48 is substituted in the expression for W, the smallest possible path length becomes

$$L = 7.5 \times 10^{16} \text{ cm.} = .025 \text{ parsec.} \qquad (3.49)$$

At the distance of the Orion Nebula, this distance would subtend an angle of 0.18, which is much smaller than the size of the bright nebulosity around θ^1 Ori C.

The actual path length through the nebula must be greater because of the great saturation of the absorption line. However, in view of the quite short minimum path found, the strong absorption of λ3889 in θ^2 Ori, with an equivalent width of 0.19 Angstroms, can still be understood even though the star is much less reddened than θ^1 Ori and probably lies in front of much of the material which is responsible for the reddening in θ^1 Ori.

Chapter IV. Two Photon Emission from the 2^3S Level in Helium

A. Fundamental Relations.

A helium atom in a 2^3S level cannot radiate its excitation energy by a single photon of any multipole order, but must undergo ionization by incident radiation, suffer a collision which changes its state, or emit two photons simultaneously and thus undergo a radiative transition to the 1^1S level. In order to compute the probability of a transition from level n to n'' with the simultaneous emission of two photons, one uses second order perturbation theory applied to transitions from n to an intermediate state n' by means of an optically allowed transition and from n' to n'' by a second optically allowed transition. The frequencies of the emitted photons are given by the relation

$$h(\nu + \nu') = \Phi_{n''} - \Phi_{n} , \tag{4.1}$$

where the Φ's are the ionization energies of the levels, the ν's denote the frequencies of the two photons, and h is Planck's constant.

Goeppert-Mayer [40] gives the probability of emission of two photons of frequencies ν and ν' from level n to n'' via the state n' as

$$w(\nu)\, d\nu = 2^{10}\pi^6\, e^4\, \nu^3\, (\nu')^3\, h^{-1}\, c^{-6} \times$$
$$\left\{ \left| \sum_{n'} \left[\frac{(\vec{r}\cdot\vec{u})_{nn'}\,(\vec{r}\cdot\vec{u})_{n'n''}}{\nu_{n'n} + \nu} + \frac{(\vec{r}\cdot\vec{u}'')_{nn'}\,(\vec{r}\cdot\vec{u}')_{n'n''}}{\nu_{n'n''} - \nu} \right] \right|^2 \right\}_{\text{average}} , \tag{4.2}$$

where $\vec{u}$ = polarization vector of the photon of frequency ν,

$\vec{u}'$ = polarization vector of the photon of frequency ν',

the subscripts n', n'' on quantities in parentheses refer to the matrix element between the levels n' and n'', and the average is to be taken over all spatial directions independently for the two photons. The sum over the connecting states n' should be understood to include integration over states in the continuum. The e, h, and c are conventional notations for the electronic charge, Planck's constant, and velocity of light, respectively. The $\nu_{n'n}$ is the frequency that a photon arising from a transition from level n' to n would have.

For transitions from the triplet states of helium to the singlet ground state, there are no optically allowed intermediate states. Both the initial and final states have optically allowed transitions only to the P states of their respective multiplicity. If strict Russell-Saunders coupling held, that is, if the Hamiltonian for the atom did not contain any terms mixing the spin and the orbital angular momentum of the electrons, the wave functions for all triplet states would be strictly orthogonal to those of all singlet states. However, the Hamiltonian does contain terms which involve $\vec{L}\cdot\vec{S}$ [41].

Let us denote the eigenfunction of a pure singlet state n, that is, of a singlet state where the amount of spin-orbit interaction is zero, as ${}^1\psi_n^{\text{pure}}$. Similarly, the wave function of a pure triplet state n will be symbolized by ${}^3\psi_n^{\text{pure}}$. The singlet wave function of the actual helium atom, with a small amount of $\vec{L}\cdot\vec{S}$ perturbation H', will be ${}^1\psi_{\text{He}}$. Then we can write

$$ {}^1\psi^{He}_n = {}^1\psi^{pure}_n + \sum_m \epsilon_{mn}\, {}^3\psi^{pure}_m \qquad (4.3) $$

where $\epsilon_{mn} \ll 1$. The value of ϵ as given by first-order perturbation theory is

$$ \epsilon_{mn} = \frac{({}^3\psi^{pure}_m \,|\, H' \,|\, {}^1\psi^{pure}_n)}{{}^3\Phi_m - {}^1\Phi_n} \quad , \qquad (4.4) $$

where $(a|Op|b)$ is the matrix element of any operator between states a and b. ${}^1\Phi_n$ is the ionization potential of the nth singlet level. The coefficient of the ${}^1\psi^{pure}$ is taken as one in equation 4.3 in order to normalize ${}^1\psi^{He}$ to first order.

We can now see that the intermediate state n' in equation 4.2 is replaced for our calculation by both the singlet and triplet P states, which are in turn slightly mixed. We will calculate the terms $(1^1S_o|\vec{r}\cdot\vec{u}|m\,{}^1P)$ and $(2^3S_1|\vec{r}\cdot\vec{u}|m^3P)$ separately and include mixing of m^3P into m^1P by calculating ϵ_{mm}. We will henceforth write ϵ_{mm} with a single subscript.

Breit and Teller [42] show by an argument that applies to helium as well as hydrogen that

$$ \left\{ \left| \sum_{n'} (\vec{r}\cdot\vec{u})_{nn'} (\vec{r}\cdot\vec{u}')_{n'n''} \left(\frac{1}{\nu_{n'n} + \nu} + \frac{1}{\nu_{n'n''} - \nu} \right) \right|^2 \right\} \text{ average} $$

$$ = \frac{1}{3} \left| \sum_m (1^1S_o|z|m^1P)(2^3S|z|m^3P)\, \epsilon_m \left(\frac{1}{\nu_{n'n} + \nu} + \frac{1}{\nu_{n'n''} - \nu} \right) \right|^2 , \qquad (4.5) $$

where for n the level 1^1S, for n' the level m^1P, and for n'' the level 2^3S have been substituted. For both the m^1P and the m^3P the quantum number m_ℓ is zero. Breit and Teller make

the equivalent requirement that only the P state wave functions which have vanishing x and y expectation values be used.

Before we can consider the quantities in equation 4.5, we will need approximate wave functions for the various 1 S and m P states. We will approximate the helium wave function by the product of a spatial part ϕ and a spin part X. The spatial part for a singlet state is symmetrical in the coordinates of the two electrons; the triplet spatial part is antisymmetrical. The spin functions have symmetries opposite from the spatial parts.

The notation $[n\ s_z(i)]$ will be used for the wave function of a hydrogenlike atom of charge z whose ith electron is in the s state with a principal quantum number of n. A similar notation will apply to p electrons except that for them $z \equiv 1$ and a superscript 1, -1, or 0 indicate the functions with eigenvalues of $\ell_z(i)$ of $+\hbar$, $-\hbar$, and 0 respectively; thus $3p^1(2)$ is the $3p$ wave function of electron 2 with $m_z = +\hbar$.

The spatial part of the 1^1S wave function is approximately

$$\phi(1^1S) = 1s_{z'}(1) \cdot 1s_{z'}(2), \tag{4.6}$$

where z' is the value of the charge which gives the minimum energy for a product wave function of this form. It can be shown [43] that $z' = 27/16$.

Similarly,

$$\phi(n^1P) = 2^{-1/2}[1s_2(1)\ np^o(z) + 1s_2(2)\ np^o(1)]. \tag{4.7}$$

Having the wave functions for the singlet states, we can compute the matrix element $(1^1S|z|n^1P)$ which appears in equation

4.5. The z operator is the sum of z(1) and z(2).

$$(1^1S|z|n^1P) = \int_{\text{all space}} dv\,(1)\,dv\,(2)\,\Big\{1\mathcal{A}^*_{z'}(1)\cdot 1\mathcal{A}^*_{z'}(2)[z(1)+z(2)]\times$$

$$[(1\mathcal{A}_2(1)\ np^o(2) + 1\mathcal{A}_2(2)\ np^o(1)]\Big\}\ , \qquad (4.8)$$

where dv(j) is a volume element of the coordinates of electron j and the asterisk indicates that the complex conjugate of the associated quantity should be used.

Since equation 4.8 is symmetrical in the coordinates of the two electrons, the value of the integral is double the contribution of the z(1) operator. The z(1) will connect only s(1) and p(1) states. Hence

$$(1^1S|z|n^1P) = 2\int_{\text{all space}} dv\,(1)\,dv\,(2)$$

$$\Big\{1\mathcal{A}^*_{z'}(1)\cdot z_1\cdot np^o(1)\cdot 1\mathcal{A}^*_{z'}(2)\cdot 1\mathcal{A}_{z'}(2) \qquad (4.9)$$

The function $1s_{z'}(1)$, with $z' = 27/16$, is given by [44]:

$$[1\mathcal{A}_{z'}] = \frac{3^{9/2}}{2^5}\ e^{-\frac{27}{16}r}\ \frac{1}{(4\pi)^{1/2}}\ . \qquad (4.10)$$

Also

$$1\mathcal{A}_2(1) = \left(\frac{1}{4\pi}\right)^{1/2}\ 2^{5/2}\ e^{-2r} \qquad (4.11)$$

and

$$np^o(1) = \left(\frac{3}{4\pi}\right)^{1/2}\ \cos\theta(1)\ {}^1R^1_{np}(r), \qquad (4.12)$$

where ${}^mR^z_n$ is the normalized radial part of the wave function of the level n,ℓ with a charge of z on the nucleus and a multiplicity of m.

From equations 4.9, 4.10, 4.11, and 4.12 we obtain

$$(1^1S|z|n^1P) = 3^{17/2}\, 2^{13/2}\, (59)^{-3} \int r^3 \cdot dr\; e^{-27/16r}\; {}^1R^1_{np}$$

$$= 5.008 \int r^3\, dr\; e^{-27r/16}\; {}^1R^1_{np} \quad . \qquad (4.13)$$

The spatial parts of the triplet wave functions are

$$\phi(2^3S) = 2^{-1/2}[2\mathcal{A}_1(1)\cdot 1\mathcal{A}_2(2) - 2\mathcal{A}_1(2)\cdot 1\mathcal{A}_2(1)] \qquad (4.14)$$

and

$$\phi(n^3P) = 2^{-1/2}[1\mathcal{A}_2(1)\; np^o(2) - 1\mathcal{A}_2(2)\; np^o(1)] \; . \qquad (4.15)$$

We have assumed in equations 4.14 and 4.15 that the shielding of the inner electron is complete, so that the n^3p levels are exactly hydrogenic.

Using equations 4.14 and 4.15 we get

$$(^3S|z|^3P) = \int dv\,(1)\; z(1) \int dv\,(2) \times$$

$$\left\{-[2\mathcal{A}_1(1)]\cdot[np^o(1)]^* \left|\; 1\;\; {}_2(2)\right|^2 \right.$$

$$\left. + [1\mathcal{A}_2(1)]\;[np^o(1)]^*\;[2\mathcal{A}_1(2)][1\mathcal{A}_2(2)]^*\right\} \; . \qquad (4.16)$$

The first term in braces is greater than the second because the integration over $dv(2)$ gives a factor of one in the first term, while only the overlapping parts of wave functions of different z and n contribute in the second. Actual substitution of values for the wave functions showed that the first term is ninety-one times the second for $n = 2$. The higher n terms should have even greater ratios between the two terms due to decreasing overlap between the wave functions of electron 2. We will neglect the second term in braces in equation 4.16 in the future.

The integrals in equation 4.16 are elementary, and the result of the integration is

$$({}^3S|z|{}^3P) = \frac{1}{\sqrt{3}}\ {}^3R_{2S,np} \quad , \tag{4.17}$$

where

$${}^mR_{n'\ell',n\ell} \equiv \int_0^\infty r^3\, dr\ {}^mR^1_{n\ell}\ {}^mR^1_{n'\ell'} \quad . \tag{4.18}$$

The quantities $R_{n'\ell',n\ell}$ for hydrogenic wave functions can be written in closed form [44], and tables exist for some values of the quantum numbers [36].

Let us define the quantities β, γ_n, and y by the relations

$$\nu_{2^3S-1^1S} \equiv \beta \cdot Ry; \tag{4.19}$$

$$\nu_{1^1S-np} \equiv \gamma_n \cdot Ry; \tag{4.20}$$

$$\beta y \cdot Ry \equiv \nu \tag{4.21}$$

where Ry is the Rydberg constant in frequency units. The variable y is clearly the fraction of the available energy which is taken by the photon of frequency ν. The probability per unit time of emitting two photons of frequencies corresponding to y and $(1-y)$ becomes

$$w(y)\, dy = \beta^5 \cdot Ry \cdot \alpha^6\, y^3(1-y)^3 \times$$

$$\left| \sum_{n'} (1^1S|z|n^1P)(2^3S|z|n^3P)\, \epsilon_n \left(\frac{1}{\gamma/\beta - y} + \frac{1}{\gamma/\beta - 1 + y} \right) \right|^2 , \tag{4.22}$$

where $\alpha = eh/2mc = 1/137.0$ is the atomic fine structure constant.

Equation 4.22 agrees with the corresponding expression for hydrogen as given by Greenstein and Spitzer [45] when the pertinent hydrogenic values $\beta = \frac{3}{4}$, $\gamma_n = 1 - \frac{1}{n^2}$, $_n = 1$, and $(1S|z|nP) = \frac{1}{\sqrt{3}} R_{1S,np}$ are inserted.

For helium, the values of the parameters γ_n and β are

$$\gamma_n = \frac{\Phi_{1S}}{(Ry)} - \frac{1}{n^2} = 1.810 - \frac{1}{n^2} \qquad (4.23)$$

$$\beta = \frac{\Phi_{1S} - \Phi_{2^3S}}{(Ry)} = 1.465. \qquad (4.24)$$

The quantities ϵ_n must be determined before further progress can be made on the two photon emission probability.

B. Mixing of the n^3P State into the n^1P State in Helium.

The perturbing terms in the Hamiltonian which will mix the spin and orbit terms are [41]:

$$\frac{H''}{\alpha^2} = \frac{z}{2}\left[\frac{\vec{s}(1)\cdot\vec{l}(1)}{r_1^3} + \frac{\vec{s}(2)\cdot\vec{l}(2)}{r_2^3}\right] - \frac{(\vec{s}(1)+\vec{s}(2))\cdot\vec{r}_{12}\times\vec{k}_{12}}{r_{12}^3}$$

$$+ \frac{1}{2}\frac{\vec{s}(1)\cdot\vec{r}_{21}\times\vec{k}(1)}{r_{12}^3} - \frac{1}{2}\frac{\vec{s}(2)\cdot\vec{r}_{12}\times\vec{k}(2)}{r_{12}^3} + \frac{\vec{s}(1)\cdot\vec{s}(2)}{r_{12}^3}$$

$$- \frac{3(\vec{s}(1)\cdot\vec{r}_{12})\,(\vec{s}(2)\cdot\vec{r}_{12})}{r_{12}^5} \,. \qquad (4.25)$$

In equation 4.25 $\vec{s}(i)$ is the spin of the ith electron, $\vec{l}(i)$ the corresponding angular momentum, $\vec{k}(i)$ the propagation vector, $\vec{r}_{12}$ the vector from electron 1 to electron 2, α the fine structure

constant as before and z the charge of the nucleus.

Let us introduce the sum of the spins $\vec{S}$ and the difference $\vec{T}$, defined by

$$\vec{s}(1) + \vec{s}(2) \equiv \vec{S} \qquad \vec{s}(1) - \vec{s}(2) \equiv \vec{T}. \tag{4.26}$$

In terms of $\vec{S}$ and $\vec{T}$, equation 4.25 becomes

$$\frac{H''}{\alpha^2} = \frac{z}{4}\left[\frac{\vec{S}\cdot\vec{\ell}_1}{r_1^3} + \frac{\vec{S}\cdot\vec{\ell}_2}{r_2^3}\right] - \frac{\vec{S}\cdot\vec{r}_{12}\times\vec{k}_{12}}{r_{12}^3} + \frac{1}{4}\,\vec{S}\cdot\vec{r}_{12}\times\vec{k}_{12} \tag{4.27}$$

$$+\frac{S^2}{4r_{12}^3} - \frac{3}{4}\frac{(\vec{S}\cdot\vec{r}_{12})}{r_{12}^5} + \frac{z}{4}\left[\frac{\vec{T}\cdot\vec{\ell}_1}{r_1^3} - \frac{\vec{T}\cdot\vec{\ell}_2}{r_2^3}\right] + \frac{\vec{T}\cdot\vec{r}_{12}\times(\vec{k}_1+\vec{k}_2)}{4r_{12}^3} - \frac{1}{4}\frac{T^2}{r_{12}^3}$$

$$+\frac{3}{4}\frac{(\vec{T}\cdot\vec{r}_{12})^2}{r_{12}^5} + \frac{1}{4}\frac{[\vec{T}\cdot\vec{S} - \vec{S}\cdot\vec{T}]}{r_{12}^3} - \frac{3}{4}\left[\frac{(\vec{T}\cdot\vec{r}_{12})(\vec{S}\cdot\vec{r}_{12})}{r_{12}^5}\right.$$

$$+\frac{3}{4}\frac{(\vec{S}\cdot\vec{r}_{12})\,(\vec{T}\cdot\vec{r}_{12})}{r_{12}^5}\,.$$

We require the matrix element of H'' between ^3P and ^1P states. The triplet is symmetric in the spin and the singlet antisymmetric, so that only terms which are antisymmetric in the spins will contribute. Therefore only terms which contain $\vec{T}$ can affect the matrix element. A similar consideration leads to the conclusion that only terms which are antisymmetrical in the spatial coordinates will be different from zero. The last four terms of equation 4.27 contribute nothing for this reason. Henceforth only the connecting part of the perturbation, designated by H', will be considered. The only important parts of equation 4.27 for our purposes will be

$$\frac{H'}{\alpha^2} = \frac{z}{4}\left[\frac{\vec{T}\cdot\vec{\ell}(1)}{r^3(1)} - \frac{\vec{T}\cdot\vec{\ell}(2)}{r^3(2)}\right] + \frac{1}{4}\,\frac{\vec{T}\cdot\vec{r}_{12}\times(\vec{k}_1+\vec{k}_2)}{r_{12}^3} \quad . \tag{4.28}$$

Since $\vec{r}_{12} \equiv \vec{r}(1) - \vec{r}(2)$, and $\vec{r}(1)\times\vec{k}(1) = \vec{\ell}(1)$,

$$\frac{H'}{\alpha^2} = \frac{z}{4}\left[\frac{\vec{T}\cdot\vec{\ell}(1)}{r_1^3} - \frac{\vec{T}\cdot\vec{\ell}(2)}{r_2^3}\right] + \frac{\vec{T}\cdot[\vec{\ell}(1)-\vec{\ell}(2)]}{4r_{12}^3} + \frac{\vec{T}(\vec{r}(1)\times\vec{k}(2)-\vec{r}(2)\times\vec{k}(1))}{4r_{12}^3}$$

The perturbation H' can mix only states of the same total angular momentum J, since the total angular momentum is a constant of the motion of the entire atom. Hence only the $^3P_1$ state will be mixed with the $^1P_1$. The situation for the total magnetic quantum number M is similar; M is a constant of the motion, and consequently only states of the same M will be mixed by H'.

Let the operator for the z-component of the spin or an electron be σ_z. Then

$$\sigma_z\alpha = +\frac{1}{2}\hbar\,\alpha$$

$$\sigma_z\beta = -\frac{1}{2}\hbar\,\beta \quad . \tag{4.30}$$

serve to define α and β. Also let

$$X_1^1 = \alpha(1)\alpha(2)$$

$$X_1^0 = 2^{1/2}[\alpha(1)\beta(2) + \beta(1)\alpha(2)]$$

$$X_1^{-1} = \beta(1)\,\beta(2) \quad . \tag{4.31}$$

The X's are the eigenfunctions of the operators S^2 and S_z; an eigenfunction of L^2 and L_z is given by equation

4.15. We can write $np^m(i)$ in terms of the normalized spherical harmonics Y_ℓ^m and the radial functions:

$$np^m(i) = R^1_{n1}\, Y^m_1(\theta_i,\phi_i) \qquad m = \pm 1, 0 \qquad (4.32)$$

The wave function for the n^3P_1 state can be expressed as a linear combination of the eigenfunctions of the operators L^2, L_z, S^2, and S_z by means of the Clebsch-Gordan coefficients. Specifically,

$$\psi_{n^3P_1} = \frac{1}{\sqrt{3}} \sum_{M=-1}^{+1} \Big[R^2_{1s}(r_1)\, R^1_{np}(r_2) \sum_{m=-1}^{+1} C^{1M}_{1m1\mu}\, Y^m_1(\theta_2)\, X^M_1 - R^2_{10}(r_2)\, R^1_{np}(r_1) \sum_{m=-1}^{+1} C^{1M}_{1n1\mu}\, Y^m_1(\theta_1)\, X^M_1\Big] , \qquad (4.33)$$

where $m + \mu = M$ in each sum and the C's are Clebsch-Gordan coefficients. In the notation used here, $C^{JM}_{LmS\mu}$ is the coefficient of the product of LS eigenfunctions of quantum numbers L, m and S,μ in the JM eigenfunction.

The vector addition of $\vec{L}$ and $\vec{S}$ in the singlet case is trivial, and the result is

$$n^1P_1 = \frac{1}{\sqrt{3}} \sum_{m=-1}^{+1} \big[R^2_{10}(r_1)\, R^1_{np}(r_2)\, Y^M_1(\theta_1) + R^2_1(r_2)\, R^1_{2p}(r_1)\, Y^M_1(\theta_1)\big]\cdot X_o \qquad (4.34)$$

where $$X_o = \frac{1}{\sqrt{2}} [\alpha(1)\beta(2) - \alpha(2)\beta(1)] \quad . \qquad (4.35)$$

We now consider terms of the form $(X^\mu_1 | \vec{T}\cdot\vec{V} | X_o)$, where $\vec{V}$ is any spatial vector. Consider only the contributions of the z components of the vectors:

$$(X_1^{\mu}|T_z \cdot V_z|X_o) = (X_1^{\mu}|V_z \cdot [s_z(1) - s_z(2)]|[\alpha(1)\beta(2) - \alpha(2)\beta(1)] \cdot \frac{1}{\sqrt{2}})$$

$$= (X_1^{\mu}|\frac{1}{2\sqrt{2}} V_z[\alpha(1)\beta(2) + \alpha(2)\beta(1) + \alpha(1)\beta(2) + \alpha(2)\beta(1)]) \quad (4.36)$$

$$= (X_1^{\mu} \frac{1}{\sqrt{2}} V_z[\alpha(1)\beta(2) + \alpha(2)\beta(1)]) \quad . \quad (4.37)$$

We can then write out the X_1^{μ} for each μ in terms of the α and β eigenfunctions and perform the integration over the spin coordinates. A similar procedure can be carried out for the x and y terms of the $\vec{T} \cdot \vec{V}$ product. The sum of the three terms turns out to be

$$(X_1^{\mu}|\vec{T} \cdot \vec{V}|X_o) = V_z \qquad (\mu = 0) \quad (4.38)$$

$$= \mp \frac{V_x \mp i V_y}{\sqrt{2}} \qquad (\mu = \pm 1) \quad . \quad (4.39)$$

A given wave function n^1P will contain small amounts of any triplet function m^3P admixed, but because of the energy difference term dividing the matrix element of the perturbation in equation 4.4 the amount of admixture from the triplet level of the same quantum number n will predominate. For the present we will discuss only mixing of levels of the same principal quantum number n.

With the definitions

$$\rho_A^M \equiv X_o \cdot Y_1^M(\theta_2) \cdot {}^1R_{1s}^2(r_1) \cdot {}^1R_{np}^1(r_2), \quad (4.40)$$

$$\rho_B^M = C_{1m1\mu}^{1M} Y_1^m(\theta_2)\, X_1^{\mu}\, {}^3R_{1s}^2(r_1)\, {}^3R_{np}^1(r_2), \quad (4.41)$$

we have

$$\psi_{n^1P_1} = \frac{1}{\sqrt{3}} \sum_{M=-1}^{+1} (\rho_A^M - \overline{\rho_A^M}) \quad (4.42)$$

and

$$\psi_{n^3P_1} = \frac{1}{\sqrt{3}} \sum_{M=1}^{+1} (\rho_B^M - \overline{\rho_B^M}), \tag{4.43}$$

where a bar over a function indicates that the electrons 1 and 2 are to be interchanged in the function. Then

$$(n^3P_1 \left| \frac{H'}{\alpha^2} \right| n^1P_1) = \frac{1}{3} \sum_{M=-1}^{+1} \left[(\rho_B^M - \overline{\rho_B^M}) \left| \frac{H'}{\alpha^2} \right| (\rho_A^M - \overline{\rho_A^M}) \right] \tag{4.44}$$

$$= \frac{1}{3} \sum_M \left[(\rho_B^M \left| \frac{H'}{\alpha^2} \right| \rho_A^M) - (\overline{\rho_B^M} \left| \frac{H'}{\alpha^2} \right| \rho_A^M) - (\rho_B^M \left| \frac{H'}{\alpha^2} \right| \overline{\rho_A^M}) + (\overline{\rho_B^M} \left| \frac{H'}{\alpha^2} \right| \overline{\rho_A^M}) \right]. \tag{4.45}$$

The coordinates of the two electrons are now interchanged in the second and last terms of equation 4.45. Since $H' = \overline{H'}$,

$$(n^3P_1 \left| \frac{H'}{\alpha^2} \right| n^1P_1) = \frac{2}{3} \sum_M \left[(\rho_B^M \left| \frac{H'}{\alpha^2} \right| \rho_A^M) - (\rho_B^M \left| \frac{H'}{\alpha^2} \right| \overline{\rho_A^M}) \right]. \tag{4.46}$$

From the definition of ρ_A^M, we see that electron 1 is in an s state and consequently that only the l_2 terms in H' will contribute to the matrix element. We then get

$$(n^3P_1 \left| \frac{H'}{\alpha^2} \right| n^1P_1) = -\frac{2}{3} \sum_M \left\{ \left(\rho_B^M \left| \left[\frac{z}{4} \frac{\vec{T} \cdot \vec{l}_2}{r_2^3} + \frac{\vec{T} \cdot \vec{l}_2}{r_{12}^3} \right] \right| \rho_A^M \right. \tag{4.47}$$

$$\left. + \left(\rho_B^M \left| \frac{\vec{T} \cdot (\vec{r}_1 \times \vec{k}_2 - \vec{r}_2 \times \vec{k}_1)}{4 r_{12}^3} \right| \overline{\rho_A^M} \right) \right\}.$$

We will designate the first and second terms of the right side of equation 4.47 as $(H'/\alpha^2)_a$ and $(H'/\alpha^2)_b$ respectively. For $(H'/\alpha^2)_a$ we make the approximation

$$\frac{\vec{l}(2)}{2r^3(2)} + \frac{\vec{l}(2)}{4r_{12}^3} \approx \frac{3}{4} \frac{\vec{l}(2)}{r^3(2)}, \tag{4.48}$$

which should be quite valid; electron 1 is considered to be in the 1s configuration in ρ_B^M and is therefore very close to the nucleus on the average. Use of equations 4.38, 4.39, 4.48, and tabulated values of the Clebsch-Gordan coefficients leads to the result

$$(\psi_{1P_1}|\frac{H'}{\alpha 2}|n^3P_1)_a = \frac{3}{2\sqrt{2}}\int_0^\infty \frac{dr_2}{r_2}\, {}^1R^1_{n1}(r_2)\, {}^3R^1_{n1}(r_2). \qquad (4.49)$$

It is clear from an inspection of $(H'/\alpha^2)_b$, the second term on the right of equation 4.47, that it is considerably smaller than $(H'/\alpha^2)_a$. The function upon which the $(H'/\alpha^2)_b$ operates, $\overline{\rho_B^M}$, represents electron 1 in the np state and electron 2 in the 1s state. When the wave function is fairly large (at $r \simeq n^2$ Bohr radii), $\vec{k}(2)$, proportional to the gradient of the wave function of electron 2, is small. It is clear that an $\vec{l}_1$ $(= \vec{r}(1) \times \vec{k}(1))$ operator would have a larger matrix element, since both the wave function and the gradient of the wave function of electron 1 are large at about n^2 Bohr radii.

As a test of the above argument, the rather laborious algebraic work necessary to determine $(H'/\alpha^2)_b$ was carried out for the case $n = 2$, for which case the ratio of the two terms should be most in favor of the second. The electron separation r_{12} was approximated by the larger of the radii $r(1)$ and $r(2)$. The result of the calculation was that

$$(\frac{H'}{\alpha 2})_b = .00062\,\frac{e^2}{a_o} = \frac{1}{41}\,(\frac{H'}{\alpha 2})_a . \qquad (4.50)$$

The second term $(H'/\alpha^2)_b$ will be neglected in the future.

The matrix element H' can now be determined from equation 4.49 if the radial portions of the np wave functions are known. The functions given by Goldberg [31] were used for the 1^1S, 2^1P, 2^3P, 3^1P, and 3^3P states, while hydrogenic wave functions were used for $n \geq 3$ for both singlets and triplets.

To calculate the ϵ_n's by equation 4.4, we only have to divide the matrix elements H'/α^2, as given by equation 4.50, by the experimental values of the energy differences of the singlet and triplet levels for the various values of n. The energy differences are tabulated by the National Bureau of Standards [45]. Table 4.1 summarizes the results of the computation. The second column gives the experimental values of $({}^3X_n - {}^1X_n)$; the third, the value of the matrix element H'/α^2 in units of e^2/a_o (where a_o is the first Bohr radius); the fourth, the dimensionless ϵ_n's.

Table 4.1. Values of the Mixing Parameter

n	${}^3X_n - {}^1X_n$ (cm^{-1})	$(n^3P_1 \lvert H'/\alpha^2 \rvert n^1P_1)$ (units of e^2/a_o)	ϵ_n
2	204.8	+0.0485	+0.00025
3	644.5	.0131	.00021
4	275.6	.0056	.00021
5	141.7	.0028	.00021
6	81.96	.0016	.00021

It should be noted that only mixing between levels of the same n has been considered. An attempt was made to obtain an estimate of the error introduced by the failure to include all levels; the values of ϵ_{m3}, the amplitude of $\psi_{m^3P_1}$ mixed into

$\psi_{3^1P_1}$ by spin-orbit interactions, were determined for the low m levels. Hydrogenic wave functions were used in the calculation. The results are given in Table 4.2 below.

Table 4.2. Mixing of $\psi_{m^3P_1}$ into $\psi_{3^1P_1}$ in Helium.

m	$(m^3P_1\|H'/\alpha^2\|3^1P_1)$	$^3X_m - {}^1X_3$	$\epsilon_{m3}/\epsilon_{33}$
2	5.7×10^{-3}	17,120 cm^{-1}	.042
4	8.4×10^{-3}	5,008 "	.095
5	6.2×10^{-3}	7,592 "	.046
6	4.9×10^{-3}	9,051 "	.032

From Table 4.2 the percentage error arising from the neglect of states of unequal principal quantum numbers can be estimated as perhaps thirty or forty percent. Our results can only be regarded as fairly rough because of this uncertainty.

C. Computation of the Mean Lifetime of the 2^3S Level in Helium

Equation 4.22 gives the probability per unit time that a helium atom in the 2^3S level will emit two photons with energies y and (1-y) times the available amount respectively. The total probability of two photon emission per unit time P is obtained by integrating W(y) dy over y, with a factor of one-half multiplying the integral since only the numbers of pairs of photons should be counted. Thus

$$P = \frac{1}{2}\int_0^1 W(y)\, dy. \qquad (4.51)$$

Now all of the quantities which appear on the right side of equation 4.22 are known, and $W(y)$ can be computed straightforwardly. The results of the computation are given in Tables 4.3 and 4.4.

A modified form of Simpson's Rule was used to carry out the numerical integration of $W(y)$. The approximation to the integral of a periodic function is the sum of the values of the function at an even number of equally spaced intervals of the argument.

The contributions of transitions via $n^3P - n^1P$ states for $n > 5$ have been neglected in computing the total probability P. Table 4.3 shows that the contribution from $n = 2$ is by far the largest, and that higher n terms fall rapidly.

The mean lifetime τ of a helium atom in the 2^3S state is simply the reciprocal of the emission probability per unit time P. From numerical integration of the values of $W(y)$ as given in Table 4.4 we obtain

$$P = 1.1 \times 10^{-5} \text{ sec}^{-1} \qquad (4.52)$$

and

$$\tau = 1/P = 9 \times 10^{5} \text{ sec} \qquad (4.53)$$

The total uncertainty in the value of P is difficult to estimate. The largest errors arise from the neglect of the mixing of singlet and triplet levels of different principal quantum number in the calculations of transitions via the low quantum number P states and from the neglect of transitions via the high P states

Table 4.3. Values of Mixing Parameter A_n.

$$A_n = (2^1S_1|z|n^1P_1)(n^3P_1|z|2^3S_1)\ \epsilon_n\left(\frac{1}{\gamma_n/\beta - y} + \frac{1}{\gamma_n/\beta - 1+y}\right)$$

and is expressed below in units of a_o^2 .

y	n	2*	3	4	5	$_nA_n$
.10,	.90	-4.35	+.53	+.09	+.03	-3.70
.20,	.80	-3.07	+.41	.08	.03	-2.56
.30,	.70	-2.54	+.36	.08	.03	-2.07
.40,	.60	-2.30	+.33	.07	.02	-1.88

---

* The minus sign arises from the fact that R^{2S} is negative for m = 2 and positive for all other values of m.

and in particular the continuum. Also the wave functions which were used in the calculation of the matrix elements were only approximate. Since the quantities which these errors affect appear squared in the expression for P, probably the value of P derived is not accurate to better than a factor of two.

The value of the probability of the two-photon emission was estimated by Breit and Teller [42] as about 10^{-6} times as large as the probability as for hydrogen, for which they estimated a probability of 7 $sec.^{-1}$ Their estimate is thus off by a factor of about sixty. A great deal of the difference in the estimates lies in the difference in the frequencies involved in the transition. Their estimate of the value of the mixing parameter was 1/2000, which is within a factor of three of the calculated value.

Table 4.4. Values of Emission Probability W(y).

y		W(y) x 10^8 (sec^{-1})	y		W(y) x 10^8 (sec^{-1})
0,	1.00	0.00			
.05,	.95	.40	.30,	.70	7.24
.10,	.90	1.84	.35,	.65	8.28
.15,	.85	3.38	.40,	.60	8.80
.20,	.80	4.90	.45,	.55	9.12
.25,	.75	6.22	.50		9.38

$$P = \frac{1}{2} \int_0^1 W(y)\, dy = 10 \sum_i W(y_i) = 1.10 \times 10^{-5}\ sec^{-1}$$

Appendix A. Coudé Calibration Plates Taken.

The calibration plates on the IIa-J emulsion were taken with Grating 46-B set at $93^{\circ}.7$ with a 200 watt frosted bulb as the light source. No "bull's eye" filter was used. A screen which passes about one-fifth of the light was occasionally used. Lamp distances were measured from the front diffuser. The correct exposure times were found to be:

Time	Screen	Lamp distance
30 sec.	-	1.5'
90 sec.	-	2.5'
3 min.	yes	1.5'
30 min.	yes	4.5'
90 min.	yes	7'

For 103a-F(3) emulsion, a Wratten #3 filter was placed over the spectrograph slit in the path of both the light source and the comparison arc. A photoflood bulb was used with the "bull's eye" filter. Grating 46-B was set at $87^{\circ}.4$. A comparison spectrum with twenty seconds of iron arc and thirty second of neon discharge was used. The exposure times were as follows:

Time	Screen	Lamp distance
3 min.	-	3.5'
9 min.	-	6'
30 min.	-	11'
180 min.	yes	10'

The 73" camera was used for all exposures.

Appendix B. Oscillator Strengths for Transitions in Hydrogen

Kupper [37] gives general formulae for quantities which he calls a^2, that are related to the $(R_{n,\ell,n',\ell'})^2$ of Chapter IV by

$$a^2 = (R_{n\ell,n'\ell'})^2 \quad (\frac{\ell_{max}}{2}) \tag{B.1}$$

where ℓ_{max} is the greater of ℓ and ℓ'. Bethe [36] expresses the oscillator strength in terms of $R_{n\ell,n',\ell'}$ as

$$f_{n\ell,n'\ell'} = \frac{1}{3} \frac{(\ell_{max})}{(2\ *+\ 1)} (\frac{\nu_{n\ell,n'\ell'}}{Ry}) (R_{n\ell,n'\ell'})^2 \tag{B.2}$$

where ℓ^* is the angular momentum quantum number of the level with smaller principal quantum number.

Substitution in equation B.2 of Kupper's formulae gave the following formulae for the transitions between the indicated levels where the principal quantum number n is understood to be larger in the higher state.

Transition	Expression for oscillator strength
3D - nF	$\frac{2^{13}\ 3^7}{5^2}\ n^8\ \frac{(n-3)^{2n-9}}{(n+3)^{2n+9}}\ \frac{(n+3)!}{(n-4)!}$
4D - nF	$\frac{2^{34}}{5^2\ 9}\ n^8\ \frac{(n-4)^{2n-10}}{(n+4)^{2n+10}}\ \frac{(n+4)!}{(n-5)!}$
4F - nG	$\frac{2^{38}}{3^2\ 5\ 7}\ n^{10}\ \frac{(n-4)^{2n-10}}{(n+4)^{2n+10}}\ \frac{(n+3)!}{(n-4)!}$

Transition	Expression for oscillator strength
5D - nF	$\frac{2^{13}\,5^{11}}{7\,9}\,n^{10}\,\frac{(n+3)!}{(n-4)!}\,\frac{(n-5)^{2n-12}}{(n+5)^{2n+12}}\,(11n^2-175)^2$
5G - nF	$\frac{2^{24}\,5^{13}}{9!\,3^3}\,n^{12}\,\frac{(n-5)^{2n-13}}{(n+5)^{2n+13}}\,\frac{(n+5)!}{(n-6)!}$
5F - nG	$\frac{2^{17}\,5^{11}}{3^3\,7^2}\,n^{10}\,\frac{(n-5)^{2n-11}}{(n+5)^{2n+11}}\,\frac{(n+4)!}{(n-5)!}$
6F - nG	$\frac{2^{24}\,6^{11}}{7\,9!}\,n^{10}\,\frac{(n-6)^{2n-14}}{(n+6)^{2n+14}}\,\frac{(n+4)!}{(n-5)!}\,(8n^2-324)^2$
7F - nG	$\frac{2^{25}\,7^{11}}{3^2 10!}\,n^{10}\,\frac{(n-7)^{2n-15}}{(n+7)^{2n+15}}\,\frac{(n+4)!}{(n-5)!}$
	$(121n^4 - 7350n^2 + 108045)^2$

The numerical results obtained from substitution in the above expressions are given in Table B.1.

Table B.1. Numerical Values of Oscillator Strengths in Hydrogen.

Transition	3D - nF	4D - nF	4F - nG	5D - nF	5G - nH
n	f_{ij}	f_{ij}	f_{ij}	f_{ij}	f_{ij}
4	1.018	-	-	-	-
5	.157	.890	1.345	-	-
6	.0539	.186	.181	.837	1.679
7	.0254	.0723	.0585	.1955	.202
8	.0144	.037	.0268	.0805	.0599
9	.00903	.0215	.0146	.0423	.0259
10	.00608	.0138	.00897	.0255	.0141
11	.00431	.00954	.00598	.0167	.00826
12	.00318	.00688	.00421	.0110	.00541
13	.00242	.00515	.00310	.0085	.00376
14	.00189	.00397	.00235	.0065	.00274
15	.00150	.00312	.00183	.0050	.00207
16	.00122	.00251	.00146	.0040	.00160
17	.00100	.00205	.00118	.0032	.00127
18	.000831	.00170	.000970	.0026	.00103
19	.000700	.00142	.000808	.0022	.00084
20	.000595	.00120	.000681	.0019	.00070
21	.000475	.00103	.000580	.0016	.00060
22	.000414	.000886	.000499	.0014	.00050
23	.000362	.00070	.000431	.0012	.00043
24	.000318	.00067	.000376	.0010	.00037
25	.000282	.00055	.000330	.009	.00033
26	.000251	.00049	.000291	.0008	.00029
27	.000222	.00044	.000238	.0006	.00025
28	.000200	.00039	.000213	.0006	.00022
29	.000181	.00035	.000192	.0005	.00020
30	.000163	.00032	.000172	.0005	.00018

Table B.1. Numerical Values of Oscillator Strengths in Hydrogen (continued)

Transition n	5F - nG f_{ij}	6F - nG f_{ij}	7F - mG f_{ij}
4	-	-	-
5	-	-	-
6	1.184	-	-
7	.229	1.1030	-
8	.0845	.2442	1.183
9	.0415	.0971	.2685
10	.0238	.0497	.1081
11	.0152	.0295	.0564
12	.0103	.01920	.0339
13	.0075	.01332	.0222
14	.0055	.00967	.0156
15	.0042	.00729	.0114
16	.0034	.00565	.00865
17	.0027	.00448	.00675
18	.0022	.00362	.00537
19	.0018	.00298	.00436
20	.0015	.00248	.00360
21	.0013	.00209	.00301
22	.0011	.00178	.00254
23	.0010	.00153	.00217
24	.0008	.00132	.001875
25	.0007	.00115	.001625
26	.0006	.00101	.00142
27	.0006	.00089	.00125
28	.0005	.00079	.001109
29	.0004	.00071	.000985
30	.0004	.00063	.000884

Appendix C. List of the Coefficients d_{ij} for Helium.

The coefficients d_{ji}, defined in equation 3.37, are given below. The subscripts i and j refer to the levels as listed in Table 3.1.

i	j	dji
3	2	2.218
4	3	2.120
5	2	2.524
5	4	.2241
6	3	22.133
7	3	.3234
7	5	.3602
8	2	1.224
8	4	.10656
8	6	.08924
8	7	.04111
9	3	8.915
9	5	2.409
9	8	.0001433
10	6	6.708
11	2	.6533
11	4	.0154
11	6	.0369
11	7	.0273
11	9	.0489
12	3	4.364
12	5	1.662
12	8	.566
12	10	.0174
13	6	2.213
13	9	1.259
14	10	2.648
15	3	2.465
15	5	.8850
15	8	.232
15	10	.0075
15	11	.152
15	13	.0137
16	6	1.045
16	9	.6287
16	12	.3552
17	10	.8623
17	13	.6976
18	6	.5825
18	9	.3581
18	12	.2107
18	15	.1245
19	10	.4042
19	13	.3439
19	16	.2311

References

[1] Sharpless, S., Astrophysical Journal, vol. 116, 251 (1952).

[2] Greenstein, J., and Henyey, L., Astrophysical Journal, vol. 86, 620 (1937).

[3] Greenstein, J., and Henyey, L., Astrophysical Journal, vol. 87, 79 (1938).

[4] Greenstein, J., and Henyey, L., Astrophysical Journal, vol. 89, 653 (1939).

[5] Wyse, A., Astrophysical Journal, vol. 95, 356 (1942).

[6] Greenstein, J., Astrophysical Journal, vol. 104, 414 (1946).

[7] Baade, W., and Minkowski, R., Astrophysical Journal, vol. 86, 823 (1937).

[8] Stebbins, J., and Whitford, A.E., Astrophysical Journal, vol. 98, 20 (1943).

[9] Stebbins, J., and Whitford, A.E., Astrophysical Journal, vol. 102, 318 (1945).

[10] Stromgren, Bengt, Astrophysical Journal, vol. 89, 526 (1939).

[11] Osterbrock, D., Astrophysical Journal, vol. 122, 238 (1955).

[12] Aller, L.H., and Bohm, D., Astrophysical Journal, vol. 105, 131 (1947).

[13] Swihart, T., Master's Thesis, University of Indiana,

[14] Cillie, G.G., Monthly Notices of the Royal Astronomical Society, vol. 96, 771 (1936).

[15] Menzel, D.H., and Baker, J.B., Astrophysical Journal, vol. 85, 330 (1937); vol. 86, 70 (1937); vol. 88, 52 (1938). For other papers in the series see Astrophysical Journal, vol. 102, 239 (1945).

[16] Goldberg, L., Astrophysical Journal, vol. 93, 244 (1941).

[17] Seaton, M.J., Monthly Notices of the Royal Astronomical Society, vol. 114, 154 (1954).

[18] Wilson, O.C., Publications of the American Astronomical Society, vol. 9, 274 (1939).

References (continued)

[19] Minnaert, M., Mulders, G.F.W., and Houtgast, J., Photometric Atlas of the Solar Spectrum, D. Schnabel, Amsterdam (1940).

[20] Minnaert, M., The Sun, ed. by G. Keiyser, University of Chicago Press, Chicago, Illinois, p. 95 (1953).

[21] Pettit, E., Astrophysical Journal, vol. 91, 159 (1940).

[22] Plaskett, H.H., Publications of the Dominion Astrophysical Observatory, vol. 2, 211 (1923).

[23] Liller, W., and Aller, L.H., Astrophysical Journal, vol. 120, 48 (1954).

[24] Morgan, W.W.,Harris, D.L., and Johnson, H.L., Astrophysical Journal, vol. 118, 92 (1953).

[25] Sharpless, S., Astrophysical Journal, vol. 116, 251 (1952).

[26] Harris, D.L., Astrophysical Journal, vol. 119, 298 (1954).

[27] Morgan, W.W., Code, A.D., and Whitford, A.E., Astrophysical Journal Supplement # 14, vol. II, 41-79 (1955).

[28] von Hoerner, S., Zeitscrift fur Astrophysik, vol. 30, 17 (1951).

[29] Whitford, A.E., Astrophysical Journal, vol. 107, 102 (1948).

[30] Plaskett, H.H., Publications of the Dominion Astrophysical Observatory, vol. 4, 187 (1928).

[31] Goldberg, L., Astrophysical Journal, vol. 90, 414 (1939).

[32] Wellmann, P., Zeitscrift fur Astrophysik, vol. 30, 71 (1951).

[33] Seaton, M.J., private communication to Dr. Donald Osterbrock.

[34] Massey, H., and Moiseiwitsch, B.L., Proceedings of the Royal Society of London A, vol. 227, 38 (1954).

[35] Hydleraas, E.A., Zeitscrift fur Physik, vol. 106, 395 (1937).

[36] Bethe, H., Handbuch der Physik, vol. 24:1, 440 (1933).

[37] Kupper, A., Annalen der Physik, vol. 86, 520 (1928).

[38] Menzel, D.H., and Baker, J.G., Astrophysical Journal, vol. 88, 52 (1938).

References (continued)

[39] Menzel, D.H., and Pekens, C.L., Monthly Notices of the Royal Astronomical Society, vol. 96, 77 (1936).

[40] Goeppert-Mayer, M., Annalen der Physik, vol. 9, 273 (1931).

[41] Inglis, D., Physical Review, vol. 61, 297 (1942).

[42] Breit, G., and Teller, E., Astrophysical Journal, vol. 91, 215 (1940).

[43] Schiff, L., Quantum Mechanics, McGraw-Hill Book Co., Inc., New York, p. 173 (1949).

[44] Pauling L., and Wilson, E.B., The Principles of Quantum Mechanics, McGraw-Hill Book Co., Inc., New York, p. 133 (1935).

[45] Moore, C.E., Atomic Energy Levels, National Bureau of Standards Circular 467, p. 4 (1949).